Lung Cancer 222 (2026) 109681

Contents lists available at ScienceDirect

Lung Cancer

journal homepage: www.elsevier.com/locate/lungcan

Research Paper

Navitoclax overcomes epithelial–mesenchymal transition-associated resistance in ALK-positive non-small cell lung cancer with rapid disease progression during alectinib treatment

Tomoka Nishimura [a], Shuta Tomida [b], Tadahiro Kuribayashi [a], Takaaki Tanaka [a], Taku Noumi [a], Masataka Taoka [a], Shunta Mori [a], Jun Nishimura [a], Ayako Morita [c], Kenji Takada [d], Naofumi Hara [d], Hiromi Watanabe [d], Kiichiro Ninomiya [b], Hisao Higo [d], Toshio Kubo [e], Kammei Rai [e], Eiki Ichihara [c], Kadoaki Ohashi [d,*], Katsuyuki Hotta [e], Yoshinobu Maeda [a], Yosuke Togashi [d,f,g,h], Go Makimoto [d,*]

[a] *Department of Hematology, Oncology and Respiratory Medicine, Okayama University Graduate School of Medicine, Dentistry and Pharmaceutical Sciences, Okayama, Japan*
[b] *Center for Comprehensive Genomic Medicine, Okayama University Hospital, Okayama, Japan*
[c] *Center for Clinical Oncology, Okayama University Hospital, Okayama, Japan*
[d] *Department of Respiratory Medicine, Okayama University Hospital, Okayama, Japan*
[e] *Center for Innovative Clinical Medicine, Okayama University Hospital, Okayama, Japan*
[f] *Department of Tumor Microenvironment, Graduate School of Medicine, Dentistry and Pharmaceutical Sciences, Okayama University, Okayama, Japan*
[g] *Advanced Research Field, Institute for Emerging Medical Innovation, Okayama University Hospital, Okayama, Japan*
[h] *Kindai University, Faculty of Medicine, Osaka, Japan*

ARTICLE INFO

Keywords:
ALK-positive NSCLC
Rapid disease progression
EMT
MAGE-A3
Navitoclax
Preclinical study

ABSTRACT

Objectives: ALK-positive non-small cell lung cancer (NSCLC) generally responds to the ALK tyrosine kinase inhibitor (TKI) alectinib; however, some patients experience rapid disease progression shortly after treatment initiation. This study investigated the molecular features underlying this clinically distinct phenotype and evaluated potential therapeutic strategies using patient-derived models.

Methods: A 68-year-old woman with ALK-positive NSCLC experienced disease progression within 1 month of first-line alectinib therapy despite an initial transient tumor response. Two resistant cell lines were established from an adrenal metastasis and a pleural effusion, respectively. Histopathological and molecular characterization was performed. The combination of ALK-TKIs and the B-cell lymphoma 2 family inhibitor navitoclax was evaluated in vitro and in vivo.

Results: Both cell lines harbored the *EML4–ALK* fusion variant 1 without secondary ALK mutations and demonstrated resistance to multiple ALK-TKIs. Transcriptomic profiling demonstrated epithelial–mesenchymal transition (EMT)-associated features in the resistant cell lines, supported by concordant immunohistochemical findings in the pretreatment specimen. Melanoma-associated antigen 3 (*MAGE-A3*) was identified as the most highly upregulated gene, and its knockdown significantly enhanced ALK-TKI sensitivity. Navitoclax combined with ALK-TKIs synergistically reduced cell viability and enhanced apoptosis in vitro, and lorlatinib plus navitoclax produced greater antitumor efficacy than either monotherapy in vivo.

Conclusion: These findings suggest that pre-existing EMT-associated features, together with MAGE-A3 upregulation and impaired apoptotic signaling, may contribute to rapid disease progression during alectinib treatment in a subset of ALK-positive NSCLC patients. Targeting apoptotic vulnerability with navitoclax in combination with ALK-TKIs warrants further investigation as a therapeutic strategy for this resistance phenotype.

* Corresponding authors at: Department of Respiratory Medicine, Okayama University Hospital 2-5-1 Shikata-cho, Kita-ku, Okayama, 700-8558, Japan.
E-mail addresses: kohashi@cc.okayama-u.ac.jp (K. Ohashi), gmakimoto5@okayama-u.ac.jp (G. Makimoto).

https://doi.org/10.1016/j.lungcan.2026.109681
Received 23 November 2025; Received in revised form 23 September 2026; Accepted 3 November 2026
Available online 13 November 2026
0169-5002/© 2026 The Author(s). Published by Elsevier B.V. This is an open access article under the CC BY license (http://creativecommons.org/licenses/by/4.0/).

1. Introduction

Targeted therapies against oncogenic drivers have significantly prolonged survival and have redefined the standards of care for patients with advanced non-small cell lung cancer (NSCLC). Despite these advances, lung cancer remains one of the most commonly diagnosed and deadliest malignancies worldwide [1]. NSCLC, which accounts for approximately 80 %–85 % of all lung cancers, frequently harbors alterations in driver oncogenes, such as the epidermal growth factor receptor (*EGFR*), Kirsten rat sarcoma viral oncogene homolog (*KRAS*), and anaplastic lymphoma kinase (*ALK*). *ALK* rearrangements are observed in 3 %–5 % of NSCLC cases [2]. Following the discovery of *ALK* rearrangements, ALK tyrosine kinase inhibitors (TKIs) have evolved into first-line therapies, progressing from crizotinib to more potent next-generation compounds [3]. Alectinib, a second-generation ALK inhibitor, has been established as a standard first-line therapy after demonstrating significantly prolonged median progression-free survival of 34.8 months (vs. 10.9 months with crizotinib) in the ALEX trial and 34.1 months (vs. 10.2 months) in the J-ALEX trial [4–7]. However, the emergence of TKI resistance remains a major therapeutic challenge [8]. Notably, a subset of patients experiences rapid disease progression shortly after the initiation of alectinib, although the underlying molecular and biological mechanisms remain incompletely understood.

Resistance mechanisms to ALK-TKIs involve both genetic and phenotypic alterations. Genetic mechanisms encompass on-target alterations, such as *ALK* amplification and secondary kinase domain mutations (e.g., G1202R and L1196M), as well as off-target bypass pathway activation, including *MET* amplification and EGFR activation [9–12]. Phenotype-associated mechanisms, such as epithelial–mesenchymal transition (EMT) and histologic transformation to small-cell or sarcomatoid phenotypes, have also been reported [13,14]. These resistance mechanisms are thought to arise through distinct evolutionary routes, including adaptive tumor cell responses to treatment pressure and the selection of pre-existing resistant subpopulations [8,15,16].

We previously established the ABC-14 and ABC-17 cell lines and patient-derived xenografts (PDXs) from a patient with ALK-positive NSCLC who initially responded to alectinib but experienced rapid disease progression within 3 months. Using these samples, we demonstrated that heterogeneous genetic features, including *MET* amplification with amphiregulin overexpression, the ALK G1202R mutation, and a high tumor mutation burden (TMB), were associated with rapid disease progression [17]. Similarly, other groups have reported that early progression during ALK-TKI therapy is frequently associated with *MET* amplification or neurofibromin 2 alterations [18]. However, studies specifically focusing on the molecular features associated with rapid disease progression remain limited, and the optimal treatment strategy has yet to be established.

In this study, we established novel patient-derived cell lines from a patient with ALK-positive NSCLC who experienced an initial radiological response followed by rapid disease progression within 1 month of alectinib initiation. We identified EMT-associated features, along with upregulation of melanoma-associated antigen 3 (MAGE-A3), in these resistant samples and observed functional evidence of impaired apoptotic signaling. Furthermore, we investigated the therapeutic potential of combining the B-cell lymphoma 2 (BCL-2) family inhibitor navitoclax with ALK-TKIs in preclinical models, thereby proposing a novel treatment strategy to overcome this resistance phenotype.

2. Materials and methods

2.1. Clinical samples and patient-derived cell lines

Two *ALK*-rearranged NSCLC cell lines, ABC-15 and ABC-16, were established from tumor specimens obtained from a 68-year-old female patient. Histopathological diagnosis and morphological findings were independently reviewed by an experienced pathologist. ABC-15 was established from a core needle biopsy of an adrenal metastasis following the development of resistance to alectinib, whereas ABC-16 was derived from pleural effusion obtained after the development of resistance to crizotinib. Tumor tissues were washed with saline, and mononuclear cells were isolated using the Ficoll-Hypaque density gradient method. The cells were cultured in Roswell Park Memorial Institute (RPMI)-1640 medium (Sigma-Aldrich, St. Louis, MO, USA) supplemented with 10 % fetal bovine serum (FBS) and 1 % penicillin/streptomycin. Stable cell lines were established after several weeks of culture. Both ABC-15 and ABC-16 cells were maintained for more than 20 passages without loss of proliferative capacity. These established cell lines were used for subsequent in vitro functional and drug sensitivity assays. Written informed consent was obtained from the patient and her family. This study was approved by the Institutional Review Board of Okayama University (approval number: 1603-066).

2.2. Cell lines and reagents

ABC-14 and H2228/CHR1 cells were established in our laboratory from patients with *ALK*-rearranged NSCLC. ABC-14 is a *MET*-amplified cell line [17]. H2228/CHR1 is an alectinib-resistant derivative generated from H2228 cells by stepwise exposure to alectinib and exhibits resistance associated with the loss of the Echinoderm microtubule–associated protein-like 4 (*EML4*)–*ALK* fusion gene [19]. PC-9 (*EGFR* exon 19 deletion, E746_A750) and HEK293T cells were obtained from the European Collection of Authenticated Cell Cultures and the RIKEN Cell Bank, respectively. H3122 (*EML4–ALK* variant 1) cells were provided by Dr. William Pao (Vanderbilt University), and H2228 (*EML4–ALK* variant 3a/b) cells were purchased from the American Type Culture Collection. All cell lines were maintained in RPMI-1640 medium supplemented with 10 % FBS and 1 % penicillin/streptomycin. Crizotinib, alectinib, ceritinib, brigatinib, lorlatinib, erlotinib, and SGX-523 were purchased from Selleck Chemicals (Houston, TX, USA). Navitoclax was obtained from Selleck Chemicals for in vitro studies and from AbMole BioScience (Houston, TX, USA) for in vivo studies.

2.3. Immunohistochemistry and histochemical analyses

Five-micrometer-thick sections were prepared from formalin-fixed, paraffin-embedded tissue blocks and mounted onto glass slides. The sections were deparaffinized using Hemo-De (FALMA, Tokyo, Japan; Cat. No. CS-1001-4) for 15 min, rehydrated with graded ethanol, and rinsed in distilled water. Antigen retrieval was performed by heating the sections at 95 °C for 10 min in 10 mmol/L sodium citrate buffer (pH 6.0) using a Pascal pressure chamber (Dako, Agilent Technologies, Denmark; Cat. No. S2800). Endogenous peroxidase activity was blocked using 0.3 % hydrogen peroxide in methanol for 5 min, followed by washing with TBS-T (0.1 % Tween 20). The sections were blocked with goat serum for 60 min at room temperature. The sections were incubated overnight at 4 °C with the following primary antibodies: anti-ALK (#3633, Cell Signaling Technology [CST], Danvers, MA, USA; 1:400, RRID: AB_11127207), anti-E-cadherin (#3195, CST; 1:500, RRID: AB_2291471), and anti-vimentin (#5741, CST; 1:500, RRID: AB_10695459). The following day, a horseradish peroxidase (HRP)-conjugated secondary antibody (Agilent Technologies, Santa Clara, CA, USA; Cat. No. K4003) was applied for 20 min at room temperature, followed by color development with 3,3′-diaminobenzidine (Agilent) and counterstaining with hematoxylin. Cell-block specimens of ABC-15 and ABC-16 were subjected to additional pathological characterization. Immunohistochemical (IHC) staining was performed using antibodies against cytokeratin 5/6 (CK5/6) (#M7237, Dako; 1:50, RRID: AB_2281083), Napsin A (#418061, Nichirei Biosciences, Tokyo, Japan; ready-to-use, RRID: AB_3752785), thyroid transcription factor 1 (TTF-1) (#790-4398, Roche Diagnostics GmbH, Mannheim, Germany; ready-to-use, RRID: AB_2335981), MUC1 (#NCL-MUC-1, Leica Biosystems, Newcastle upon Tyne, UK; 1:100, RRID: AB_442111), and MUC5AC

(#NCL-MUC-5AC, Leica Biosystems, 1:100, RRID: AB_442113). Periodic acid–Schiff staining was performed on the cell-block sections. Stained slides were imaged using a BZ-8100 microscope (Keyence, Osaka, Japan).

2.4. RNA extraction and detection of the EML4–ALK fusion gene

Total RNA was extracted using an RNeasy Mini Kit (QIAGEN, Venlo, The Netherlands), according to the manufacturer's protocol. The *EML4–ALK* fusion gene was detected using the SuperScript III One-Step Reverse Transcription Polymerase Chain Reaction (RT-PCR) System with Platinum Taq High Fidelity (Thermo Fisher Scientific, Waltham, MA, USA). The resulting RT-PCR amplicons were subsequently subjected to Sanger sequencing to determine the specific fusion variant by analyzing the breakpoint region between *EML4* and *ALK*. In the same cDNA-based analysis, PCR amplicons covering the ALK kinase domain, including the region encoding Gly1202, were subjected to direct Sanger sequencing to assess secondary *ALK* mutations. The Gly1202 region was covered by primer set No. 3, and primer information is provided in Supplementary Table S1A.

2.5. Cell proliferation assay

Cell proliferation was evaluated using a modified 3-[4,5-dimethylthiazol-2-yl]-2,5-diphenyltetrazolium bromide (MTT) assay. Cells were seeded into 96-well plates at a density of 1500–4000 cells per well and treated with the indicated drugs for 96 h. After adding MTT, the plates were incubated for 4 h. To dissolve the formazan crystals, a mixture of 2-propanol and hydrochloric acid (50:1) was added to each well. Absorbance was measured at 570 nm using a microplate reader.

2.6. Crystal violet staining

The cells were seeded in 6-well plates at a density of 60,000 cells per well. Three days after seeding, the cells were treated with the indicated drugs. Four days after the drug treatment, the cells were fixed with 10 % formalin for 10 min, stained with crystal violet solution (Sigma-Aldrich) for 10 min, and rinsed with distilled water. Subsequently, the plates were air-dried overnight at room temperature.

2.7. Western blotting analysis

For Western blot analyses involving drug treatment, cells were treated with the indicated drugs at the concentrations and durations specified in the corresponding figure legends before protein extraction. The cells were washed with phosphate-buffered saline (PBS) and lysed on ice for 30 min in radioimmunoprecipitation assay buffer containing 50 mM Tris(hydroxymethyl)aminomethane hydrochloride (pH 7.4), 150 mM sodium chloride, 1 % Triton X-100, 0.1 % sodium dodecyl sulfate (SDS), 1 mM EDTA, 1 mM ethylene glycol-bis(2-aminoethyl ether)-N,N,N',N'-tetraacetic acid, 10 mM β-glycerophosphate, 10 mM sodium fluoride, 1 mM sodium orthovanadate, and cOmplete EDTA-free Protease Inhibitor Cocktail Tablets (#04693132001, Roche). Lysates were centrifuged at 15,000 rpm for 30 min at 4 °C, and the supernatants were collected. Proteins were separated using SDS-polyacrylamide gel electrophoresis and transferred onto polyvinylidene fluoride membranes. The membranes were blocked with 5 % skim milk or 5 % bovine serum albumin (Sigma-Aldrich) in TBST for 1 h at room temperature, followed by overnight incubation at 4 °C with primary antibodies. After incubation with HRP-conjugated anti-rabbit IgG secondary antibodies (CST), chemiluminescent signals were detected using ECL Plus (Cytiva, Marlborough, MA, USA) and visualized using an ImageQuant 800 system (Cytiva). All primary antibodies were obtained from CST and used at the manufacturer's recommended dilutions: EGFR (#2232, RRID: AB_331707) and phospho-EGFR (Tyr1068; #3777, RRID: AB_2096270), ALK (#31278, RRID: AB_2799004) and phospho-ALK (Tyr1604; #9687, RRID: AB_10949971), STAT3 (#4904, RRID: AB_331269), and phospho-STAT3 (Tyr705; #9145, RRID: AB_2491009), AKT (#9272, RRID: AB_329827) and phospho-AKT (Ser473; #9271, RRID: AB_329825), ERK1/2 (#9102, RRID: AB_330744) and phospho-ERK1/2 (Thr202/Tyr204; #9101, RRID: AB_331646), E-cadherin (#3195, RRID: AB_2291471), vimentin (#5741, RRID: AB_10695459), ZEB1 (#3396, RRID: AB_1904164), MAGE-A3 (#38896, RRID: AB_2799142), BIM (#2933, RRID: AB_1030947), BCL-2 (#4223, RRID: AB_1903909), BCL-xL (#2764, RRID: AB_2228008), MCL-1 (#5453, RRID: AB_10694494), PARP (#9532, RRID: AB_659884) and cleaved PARP (#5625, RRID: AB_10699459), caspase-3 (#9662, RRID: AB_331439), cleaved caspase-3 (#9661, RRID: AB_2341188), p53 (#9282, RRID: AB_331476), and GAPDH (#2118, RRID: AB_561053). Western blot band intensities were quantified using Fiji/ImageJ software (National Institutes of Health, Bethesda, MD, USA). Phosphorylated protein levels were normalized to the corresponding total protein levels and then normalized to the untreated control. Cleaved PARP and cleaved caspase-3 levels were normalized to total PARP and total caspase-3 levels, respectively. MAGE-A3 expression was normalized to GAPDH and then normalized to the untreated control. Quantification was performed using the number of independent experiments indicated in the corresponding figure legends.

2.8. Receptor tyrosine kinase array assay

The phosphorylation profiles of receptor tyrosine kinases were evaluated using the Human Phospho-Receptor Tyrosine Kinase Array Kit (ARY001B; R&D Systems, Minneapolis, MN, USA). All procedures were conducted according to the manufacturer's protocol, and signal detection was performed using an ImageQuant LAS-4000 imaging system (Cytiva).

2.9. DNA extraction, MET copy number determination, and TP53 mutation analysis

DNA was extracted using the QIAamp DNA Mini Kit (QIAGEN), according to the manufacturer's instructions. *MET* gene copy number was assessed by quantitative real-time PCR (qPCR) using TaqMan probes and primers. PCR amplification was performed using a LightCycler 96 System (Roche), and the copy number was calculated based on a standard curve. Quantitative values are expressed as the ratio of *MET* to the endogenous control gene *GAPDH*. These analyses were performed based on previously described methods [20]. Primer information is provided in Supplementary Table S1B.

For TP53 mutation analysis, genomic DNA was amplified by PCR using primer sets and PCR conditions described in the International Agency for Research on Cancer protocol for the detection of TP53 mutations by Sanger sequencing [21]. PCR products were subjected to direct Sanger sequencing, and the obtained electropherograms were analyzed to identify TP53 sequence alterations.

2.10. RT-qPCR analysis

Total RNA was extracted using an RNeasy Mini Kit (QIAGEN) according to the manufacturer's instructions. Complementary DNA was synthesized from total RNA using the PrimeScript RT reagent Kit (Perfect Real Time, Takara Bio Inc., Shiga, Japan). Reverse transcription–quantitative polymerase chain reaction (RT-qPCR) was performed using TB Green Premix Ex Taq II (Tli RNaseH Plus, Takara Bio Inc.) on a real-time PCR system. Gene expression levels of *MAGE-A3* and EMT-related markers, including cadherin 1 (*CDH1*), vimentin (*VIM*), and zinc finger E-box-binding homeobox 1 (*ZEB1*) were quantified using gene-specific primers (Perfect Real Time Primer Set, Takara Bio Inc.; MAGE-A3, HA327286; GAPDH, HA067812; CDH1, HA288970; VIM, HA283325; ZEB1, HA156866), and relative mRNA expression levels were calculated using the ΔCt method, with *GAPDH* as an internal

control, and expressed as $2^{-\Delta Ct}$ values.

2.11. Combination index analysis

ABC-15 and ABC-16 cells were seeded at a density of 2500 cells per well in 96-well plates and treated with combinations of the ALK inhibitors alectinib, crizotinib, lorlatinib, and navitoclax. The drugs were combined at fixed ratios of 1:1, 2:1, and 4:1 (constant-ratio design) and incubated for 96 h. Cell viability was assessed using the MTT assay. Drug–drug interactions were evaluated using the Chou–Talalay median-effect method [22]. Fractional cytotoxicity data were used to calculate the Combination Index (CI) values using the CompuSyn software [23] (CompuSyn Inc., Paramus, NJ, USA). In the Fa-CI plots generated by CompuSyn, the x-axis represents the fraction affected (Fa) and the y-axis indicates the corresponding CI value. CI values were interpreted as follows: CI < 1 indicates synergy, CI $= 1$ indicates an additive effect, and CI > 1 indicates antagonism.

2.12. Apoptosis analysis using flow cytometry (Annexin V/7-AAD staining)

ABC-15 and ABC-16 cells were treated with lorlatinib (1 μM), navitoclax (500 nM), or a combination of both for 72 h, followed by apoptosis analysis. The in vitro drug concentrations were selected based on preliminary dose–response experiments and a previous study [24]. After treatment, the cells were washed with PBS and stained using the PE Annexin V Apoptosis Detection Kit with 7-AAD (BioLegend, San Diego, CA, USA; Cat. No. 640934), according to the manufacturer's instructions. Stained samples were analyzed using a MACSQuant flow cytometer (Miltenyi Biotec, Bergisch Gladbach, Germany). The proportion of early apoptotic (Annexin V-PE^+/7-AAD^-) cells was quantified. The data were analyzed using FlowJo version 10 (TreeStar, Ashland, OR, USA). The experiments were performed using three independent biological replicates.

2.13. Small interfering RNA transfection

Gene knockdown experiments targeting *MAGE-A3* and *ZEB1* were performed using small interfering RNA (siRNA) transfection. ABC-15 and ABC-16 cells were seeded in 6-well plates at a density of 3.0×10^5 cells/well. Transfection was carried out using Lipofectamine RNAiMAX (Thermo Fisher Scientific; Cat. No. 13778030) according to the manufacturer's instructions. Two predesigned siRNAs specific for *MAGE-A3* (QIAGEN, SI04288907 and SI04248944; Cat. No. 1027416) and two predesigned siRNAs targeting *ZEB1* (QIAGEN, SI04905089 and SI04368301; Cat. No. 1027416) were used at a final concentration of 10 nM. A non-targeting control siRNA (QIAGEN; Cat. No. 1027280) was included as the negative control. For cell proliferation assays, cells were treated with the indicated drugs at the time of transfection and incubated for 96 h. For RNA extraction and Western blot analyses, cells were treated with the indicated drugs 48 h after transfection and incubated for an additional 24 h before sample collection.

2.14. Xenograft model

Six-week-old female BALB/c nude mice (BALB/c-nu/nu) were purchased from Jackson Laboratory Japan, Inc. (Yokohama, Japan). To establish a subcutaneous xenograft model, 5×10^6 ABC-15 or ABC-16 cells suspended in a 1:1 mixture of PBS and Matrigel matrix (Corning, Glendale, AZ, USA; Cat. No. 356237) were injected into both flanks of each mouse. When the tumor volumes reached approximately 250 mm^3, the mice were randomly assigned to four groups (n = 3–6 per group): vehicle, lorlatinib (10 mg/kg), navitoclax (80 mg/kg), and lorlatinib plus navitoclax. These dose levels were selected with reference to previous preclinical studies [24,25]. Lorlatinib and/or navitoclax was administered by oral gavage once daily for 5 days per week, over a 28-day period. Tumor volumes were measured twice weekly using digital calipers and were calculated using the following formula: tumor volume = length × $(\text{width})^2 \times 0.5$. The mice were euthanized if tumor volumes exceeded 2000 mm^3 or if they showed signs of distress or impaired mobility. At the end of the study, all remaining mice were euthanized, and the tumors were excised for further analysis. All animal experiments were approved by the Animal Care and Use Committee of Okayama University (OKU-2023619).

2.15. RNA sequencing and transcriptomic analysis

Total RNA was extracted from ABC-15, ABC-16, H3122, and H2228 cells using the RNeasy Mini Kit (QIAGEN) according to the manufacturer's protocol. RNA sequencing was outsourced to a commercial service. FASTQ sequence data were analyzed using CLC Genomics Workbench (QIAGEN Digital Insights), which generated transcripts per million (TPM) values that were used for visualization and downstream analyses. Differential expression analysis was also performed by comparing ABC-15 and ABC-16 cells with the ALK-TKI-sensitive control cell lines H3122 and H2228. Upregulated genes were ranked based on log2 fold change and adjusted p-values.

Gene set enrichment analysis (GSEA) was performed using the Hallmark, KEGG, Reactome, Gene Ontology biological process, and C2 curated gene set collections from the Molecular Signatures Database (MSigDB, v2026.1.Hs). Enrichment results were evaluated using normalized enrichment scores (NES), nominal p-values, and false discovery rate (FDR) q-values. GSEA results are provided in Supplementary Table S2. Hierarchical clustering and heatmap visualization of EMT-related genes were performed using R software (version 4.3.1; R Foundation for Statistical Computing, Vienna, Austria) with the pheatmap package in RStudio (version 2025.05.1 + 513; Posit Software, PBC). Log2 TPM values were converted to Z-scores across all samples before visualization.

EMT scores were calculated from RNA-seq data using predefined epithelial and mesenchymal marker genes. The EMT score for each sample was defined as the mean Z-score of mesenchymal marker genes minus that of epithelial marker genes, with higher scores indicating a more mesenchymal phenotype. The EMT-related genes and Z-score-normalized expression values used for this analysis are provided in Supplementary Table S3. Log2 fold changes and p-values of selected EMT- and apoptosis-related genes are provided in Supplementary Table S4.

2.16. Statistical analyses

Statistical analyses were performed using GraphPad Prism version 10.4 (GraphPad Software, San Diego, CA, USA), and comparisons between two groups were performed using an unpaired two-tailed Student's *t*-test or Wilcoxon rank-sum test, as appropriate. For analyses involving multiple independent groups, one-way analysis of variance (ANOVA) followed by Tukey's post hoc test was applied. A p-value < 0.05 was considered statistically significant.

2.17. Data availability statement

The datasets generated and analyzed during the current study are available in this article and its supplementary information files. The RNA sequencing data have been deposited in the Gene Expression Omnibus (GEO, NCBI) under accession number GSE311658. Raw data derived from human samples are not publicly available due to privacy and ethical restrictions but may be made available in de-identified form by the corresponding author upon reasonable request.

3. Results

3.1. Clinical course and establishment of cell lines

A 68-year-old female patient with no history of smoking was diagnosed with advanced-stage ALK-positive lung adenocarcinoma with bilateral adrenal metastases (Fig. 1A). At initial diagnosis, ALK positivity was confirmed by immunohistochemistry using the Ventana ALK (D5F3) assay, a companion diagnostic approved by the Pharmaceuticals and Medical Devices Agency in Japan, and further genomic testing using clinical specimens was not performed. Alectinib treatment was initiated at 300 mg twice daily (600 mg/day), the approved standard dose in Japan [6]. The treatment effectively reduced the size of both the primary tumor and the metastatic lesions within 2 weeks of initiation. However, by 4 weeks after treatment initiation, the right adrenal metastasis had enlarged rapidly, exceeding 9 cm, despite continued regression of the primary lung lesion (Fig. 1B), indicating a highly discordant and aggressive progression pattern. Histopathological findings at diagnosis and from the adrenal metastasis are shown in Fig. 1C. ALK immunohistochemistry was diffusely positive in both specimens. The available biopsy specimens showed poorly differentiated tumor morphology with marked nuclear pleomorphism; however, a diagnostically definable spindle-cell or tumor giant-cell component could not be confirmed in the limited biopsy material (Fig. 1C). The patient subsequently received carboplatin (AUC 5) plus pemetrexed (500 mg/m^2) for 1 month; however, disease progression was once again observed. The treatment was then switched to crizotinib (500 mg/day), which was the only available ALK-TKI treatment option at that time and was considered feasible given the patient's deteriorating performance status. However, the disease continued to progress after 1 month. Alectinib rechallenge was performed for a further month, but no clinical benefit was achieved, and the patient died approximately 4 months after the initiation of alectinib treatment.

Two patient-derived cell lines were established from this patient: ABC-15 from a biopsy of the right adrenal metastasis obtained at progression after 1 month of alectinib treatment and ABC-16 from malignant pleural effusion collected after carboplatin plus pemetrexed followed by crizotinib treatment. Stereomicroscopic examination revealed that both cell lines exhibited an elongated morphology with a sparse cell arrangement, distinct from the epithelial cobblestone pattern. ALK immunohistochemistry revealed cytoplasmic positivity in both cell lines (Fig. 1D). Sanger sequencing of the RT-PCR amplicons confirmed the canonical *EML4–ALK* variant 1 in both ABC-15 and ABC-16 cells, with a junction between *EML4* exon 13 and *ALK* exon 20 (Supplementary Fig. S1A). In cell-block specimens, TTF-1, Napsin A, and CK5/6 were negative in both cell lines. Cytomorphological examination showed tumor cells with eccentrically located nuclei and intracytoplasmic vacuoles. PAS staining showed focal intracytoplasmic positivity in a subset of tumor cells, and MUC1 and MUC5AC were focally expressed in both cell lines (Supplementary Fig. S1B). Taken together, these results do not contradict the adenocarcinoma subtype.

3.2. No detectable ALK secondary mutations or dominant MET/EGFR bypass activation

To evaluate ALK-TKI sensitivity, MTT assays were performed on ABC-15 and ABC-16 cells. Both cell lines exhibited reduced sensitivity to alectinib, crizotinib, ceritinib, brigatinib, and lorlatinib (Fig. 2A), with only modest, dose-dependent decreases in cell viability at higher concentrations. Cell viability remained above 50 % across the tested concentration range, precluding IC50 determination. In contrast, the ALK-TKI-sensitive cell line H3122 showed dose-dependent growth inhibition with calculable IC50 values (Supplementary Fig. S2A). Western blotting was performed to assess the effect of ALK-TKIs on downstream signaling. Phosphorylation of ALK and its key effectors, including STAT3, AKT, and ERK1/2, was partially attenuated following treatment with each inhibitor (Fig. 2B). Statistically significant reductions were observed for pERK1/2 across all three ALK-TKIs in ABC-15 cells, and for pSTAT3 and pAKT under lorlatinib treatment in ABC-16 cells; other molecules showed a downward trend that did not reach statistical significance (Supplementary Fig. S2B). This difference may reflect the distinct anatomical origins and treatment histories of the two cell lines. In contrast, under the same treatment conditions, treatment with alectinib, crizotinib, or lorlatinib produced more pronounced reductions in pALK, pSTAT3, pAKT, and pERK1/2 in H3122 cells than in ABC-15 and ABC-16 cells (Supplementary Fig. S2C). These findings indicate that ALK-TKI treatment induced partial attenuation of ALK downstream signaling in both cell lines, though the extent of inhibition was incomplete and variable.

Direct sequencing of the ALK kinase domain revealed no detectable secondary mutations, including G1202R, one of the most commonly detected *ALK* resistance mutations after second-generation ALK-TKI treatment [10]. Sanger sequencing confirmed that ABC-15 and ABC-16 retained the wild-type codon GGA corresponding to Gly1202, with no evidence of a c.3604G>A (G1202R) substitution (Supplementary Fig. S2D). Together with the signaling data, these findings do not support a major role for detectable *ALK* secondary mutations in ABC-15 and ABC-16. In addition, fusion transcript analysis based on RNA sequencing data from ABC-15 and ABC-16 supported the presence of an ALK fusion transcript but did not identify other apparent oncogenic fusion events that could explain the rapid disease progression.

To investigate bypass signaling, we performed a receptor tyrosine kinase array. No marked activation of MET or EGFR was detected in any of the cell lines (Fig. 2C). In line with this, qPCR analysis revealed no *MET* amplification in ABC-15 or ABC-16 cells, in contrast to the previously reported *MET*-amplified ABC-14 cells (Supplementary Fig. S2E) [17]. Next, we tested whether bypass inhibition could restore sensitivity using a single agent or combination treatment with alectinib (ALK-TKI), crizotinib (ALK/MET inhibitor), erlotinib (EGFR-TKI), and SGX-523 (MET inhibitor). None of these combination treatments produced further suppression versus alectinib monotherapy (Fig. 2D). Collectively, these findings do not support a major role for MET- or EGFR-mediated bypass activation in resistance to ALK-TKIs in ABC-15 or ABC-16 cells.

3.3. EMT-associated transcriptional features in ALK-TKI-resistant cells

To comprehensively characterize the gene expression changes associated with ALK-TKI resistance, RNA sequencing was performed on ABC-15 and ABC-16 cells compared with ALK-TKI-sensitive cell lines (H2228 and H3122). GSEA using the Hallmark gene set collection from the MSigDB revealed significant enrichment of the Hallmark EMT gene set in ABC-15 and ABC-16 cells (Fig. 3A). Enrichment plots supported enrichment of EMT-related transcriptional programs in resistant ABC-15 and ABC-16 cell lines (Fig. 3B). A heatmap of 19 EMT-related genes showed preferential expression of epithelial markers in sensitive cells and higher expression of mesenchymal markers in resistant cells (Fig. 3C). Given the biological link between p53 inactivation and EMT features [26], we also evaluated the status of TP53 in these models. Molecular analyses identified a *TP53* exon 10 frameshift mutation (c.997dupC) in both ABC-15 and ABC-16 cells. Consistent with this genomic alteration, p53 protein expression was reduced in both resistant cell lines compared with H2228 cells (Supplementary Fig. S3A and S3B). To quantitatively assess EMT-associated transcriptional features, EMT scores were calculated as the mean Z-score of mesenchymal marker genes minus the mean Z-score of epithelial marker genes. ABC-15 and ABC-16 exhibited higher EMT scores than the ALK-TKI-sensitive cell lines, consistent with a more mesenchymal transcriptional profile (Supplementary Fig. S3C and Supplementary Tables S3A and S3B). To further assess the robustness of EMT enrichment, complementary GSEA analyses using KEGG, Reactome, Gene Ontology biological process, and C2 curated gene set collections were performed. Consistent with the

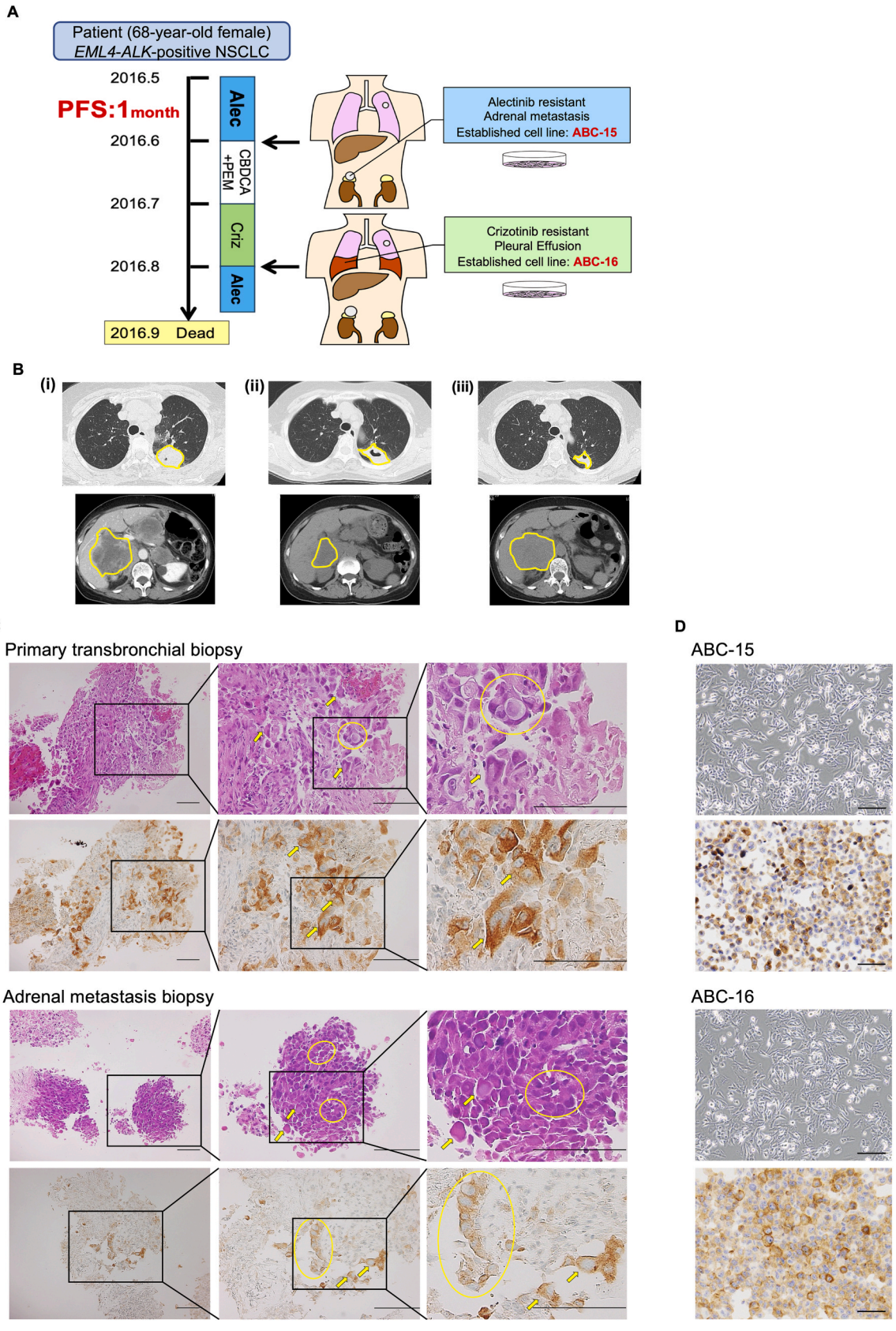

(caption on next page)

Fig. 1. Clinical course of the patient and derivation of the ABC-15 and ABC-16 cell lines. A. Clinical timeline of a patient with ALK-positive lung adenocarcinoma showing the treatment history and timing of cell line derivation. ABC-15 was derived from an adrenal metastasis after progression on alectinib, and ABC-16 was derived from pleural effusion after disease progression during crizotinib treatment. B. Computed tomography images obtained at (i) baseline before initiation of first-line alectinib, (ii) 2 weeks after initiation of alectinib, and (iii) 4 weeks after treatment initiation. Primary lung lesions are shown in the upper panels, and adrenal metastatic lesions are shown in the lower panels. Yellow outlines indicate the tumor lesions. C. The primary transbronchial biopsy specimen obtained at diagnosis and the adrenal metastasis biopsy specimen obtained during rapid disease progression on alectinib treatment were stained with hematoxylin and eosin (H&E) (upper panels) and subjected to immunohistochemistry (IHC) for ALK (lower panels). Yellow arrows indicate eccentric nuclei, whereas yellow circles indicate lumen-like spaces. Scale bars: 100 μm. D. Stereomicroscopic images (upper panels) and ALK immunohistochemistry (lower panels) of ABC-15 and ABC-16 cells. Scale bars: 100 μm. Abbreviations: Alec, alectinib; CBDCA, carboplatin; PEM, pemetrexed; Criz, crizotinib; meta, metastasis; PFS, progression-free survival. (For interpretation of the references to colour in this figure legend, the reader is referred to the web version of this article.)

Hallmark analysis, EMT-associated signatures were reproducibly identified across multiple databases and represented the most consistently enriched biological programs among those examined (Supplementary Table S2).

To determine whether these transcriptomic changes correlated with alterations at the protein level, Western blot and IHC analyses of EMT markers were performed using PC-9 (epithelial) and HEK293T (mesenchymal) cells as controls. Western blot analysis revealed that both ABC-15 and ABC-16 cells exhibited elevated vimentin expression and a decrease in E-cadherin expression, consistent with mesenchymal features (Fig. 3D). This mesenchymal protein profile was further confirmed by IHC analysis of the established cell lines (Fig. 3E and Supplementary Fig. S3D). To evaluate the clinical relevance of these in vitro findings, we next examined patient-derived tissues via IHC. Consistent with the in vitro findings, increased vimentin expression and decreased E-cadherin expression were detected in both the diagnostic biopsy specimen obtained before alectinib treatment and the adrenal metastasis specimen obtained at the time of resistance (Fig. 3E), indicating that EMT-associated features were present in the patient tumor before treatment and remained detectable at disease progression. Taken together, these findings indicate that EMT-associated features reflect intrinsic tumor biology rather than a culture-induced artifact.

3.4. *ZEB1 knockdown partially reverses EMT-associated features and reduces cell viability*

To investigate the functional relevance of EMT-associated features in ALK-TKI resistance, we focused on ZEB1, a key transcription factor significantly upregulated in our RNA-seq analysis (Supplementary Table S4). siRNA-mediated knockdown of ZEB1 in ABC-15 and ABC-16 cells was confirmed by RT-qPCR and Western blotting (Supplementary Fig. S4 and Fig. 4A). ZEB1 knockdown partially reversed EMT-associated features, as evidenced by increased E-cadherin expression at both the protein and mRNA levels, whereas vimentin expression remained largely unaltered (Fig. 4A, 4B). Notably, ZEB1 knockdown also increased BIM expression, a pro-apoptotic BH3-only protein (Fig. 4A). MTT assays demonstrated that ZEB1 knockdown significantly reduced cell viability in both resistant cell lines in the absence of lorlatinib (Fig. 4C), although a downward trend observed under lorlatinib treatment did not reach statistical significance. These findings suggest that ZEB1 contributes to the survival of resistant cells; however, ZEB1 knockdown was insufficient to fully restore lorlatinib sensitivity, suggesting that additional resistance mechanisms operate in parallel.

3.5. *MAGE-A3 contributes to the survival of resistant cells with EMT features*

To further explore the candidate genes associated with ALK-TKI resistance, we analyzed gene expression changes in the resistant ABC-15 and ABC-16 cell lines. This analysis identified *MAGE-A3* as the most highly upregulated gene (Fig. 5A and Supplementary Fig. S5A). Consistent with the RNA-seq data, RT-qPCR analysis confirmed significantly higher *MAGE-A3* mRNA expression in ABC-15 and ABC-16 cells than in H3122 cells (Supplementary Fig. S5B). Western blotting confirmed elevated MAGE-A3 protein levels in both resistant cell lines (Fig. 5B).

Given that previous reports have suggested a role for *MAGE-A3* in tumor progression and survival-related signaling pathways [27], we investigated its functional involvement in resistant cells. Two independent siRNAs targeting *MAGE-A3* effectively reduced *MAGE-A3* expression in both ABC-15 and ABC-16 cells, as confirmed by RT-qPCR (Supplementary Fig. S5C). We then assessed whether *MAGE-A3* knockdown affected lorlatinib sensitivity. The MTT assay demonstrated that siRNA-mediated knockdown of MAGE-A3 alone significantly reduced cell viability in the absence of lorlatinib, and its combination with lorlatinib led to further suppression of cell growth in both ABC-15 and ABC-16 cells (Fig. 5C). We next examined EMT markers and apoptosis-related signaling following *MAGE-A3* suppression. *MAGE-A3* knockdown did not restore E-cadherin expression compared with *ZEB1* knockdown (Fig. 5D and Supplementary Fig. S5D), suggesting that MAGE-A3 has a minimal impact on the EMT phenotype. *MAGE-A3* knockdown alone did not consistently reduce phosphorylation of ALK downstream signaling molecules, including AKT, ERK1/2, and STAT3. Under lorlatinib treatment, however, phosphorylation of AKT and ERK1/2 appeared to be more strongly reduced in *MAGE-A3*-knockdown cells than in control siRNA-treated cells (Fig. 5E). In addition, BIM expression was increased following *MAGE-A3* knockdown and appeared to be further enhanced by lorlatinib treatment (Fig. 5F). These findings suggest that MAGE-A3 may contribute to the survival of these resistant cells and modulate their response to lorlatinib.

3.6. *Navitoclax enhances the antitumor effects of ALK-TKIs in EMT-associated resistant cells*

Because navitoclax enhances apoptosis in EMT-driven EGFR-TKI-resistant lung cancer cells [24], we evaluated the effects of combining navitoclax with ALK-TKIs in ABC-15 and ABC-16 cell lines. MTT assays demonstrated that the combination treatment with navitoclax and ALK-TKIs (alectinib, crizotinib, or lorlatinib) significantly reduced cell viability compared with treatment with either agent alone (Fig. 6A). This result was confirmed by crystal violet staining, which showed a comparable decrease in cell density (Supplementary Fig. S6A). CI analysis using the Chou–Talalay method yielded CI values consistently below 1 across multiple concentrations, confirming synergistic interactions between navitoclax and all tested ALK-TKIs (Fig. 6B and Supplementary Fig. S6B). Navitoclax or its combination with lorlatinib did not significantly affect MAGE-A3 expression in ABC-15 and ABC-16 cells (Supplementary Fig. S6C).

In contrast, no clear combinatorial effect was observed in H2228/CHR1 cells [19], which exhibit loss of ALK protein expression, or in ABC-14 cells with MET amplification [17], neither of which exhibited EMT-associated features (Supplementary Fig. S6D). These findings suggest an association between EMT-associated features and sensitivity to navitoclax in a subset of resistant models.

To further characterize signaling and apoptotic alterations, Western blotting analysis was performed. ALK-TKI monotherapy partially suppressed the phosphorylation of STAT3, AKT, and ERK1/2, whereas navitoclax alone had minimal effects on downstream signaling. Combination treatment did not further suppress downstream signaling

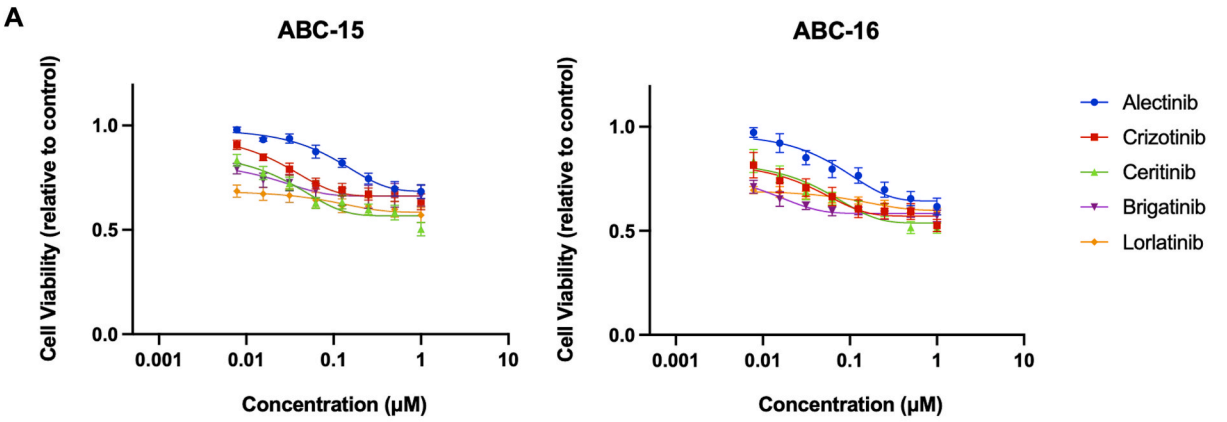

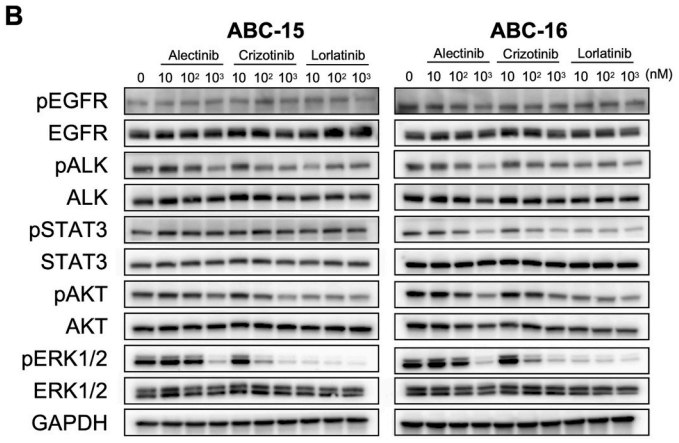

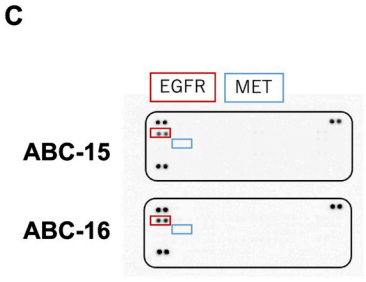

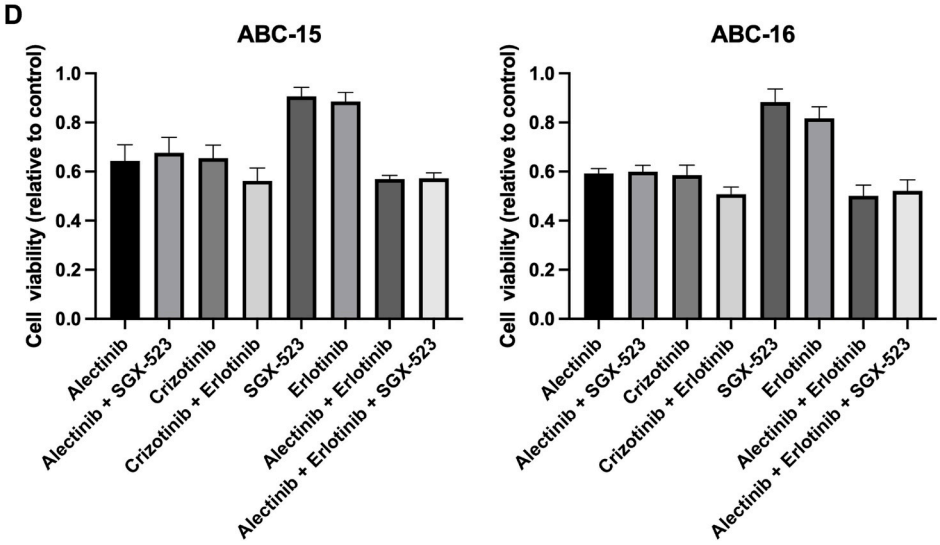

Fig. 2. Characterization of ALK-TKI resistance in ABC-15 and ABC-16 cells. A. ABC-15 and ABC-16 cells were treated with ALK-TKIs (alectinib, crizotinib, ceritinib, brigatinib, or lorlatinib) at the indicated concentrations for 96 h, after which the cell viability was assessed using the MTT assay. Data are presented as the mean ± SE of three independent experiments. B. Western blot analysis of phosphorylated and total EGFR, ALK, STAT3, AKT, and ERK1/2 in ABC-15 and ABC-16 cells following treatment with increasing concentrations of alectinib, crizotinib, or lorlatinib (10, 100, and 1000 nM) for 4 h. C. Phospho-receptor tyrosine kinase (RTK) array analysis of ABC-15 and ABC-16 cells cultured in drug-free medium for 4 days. D. ABC-15 and ABC-16 cells were treated with alectinib (ALK-TKI), crizotinib (ALK/MET inhibitor), erlotinib (EGFR-TKI), or SGX-523 (MET inhibitor), either alone or in combination, each at 1 μM for 96 h, after which cell viability was assessed using the MTT assay. Data are presented as the mean ± SE of three independent experiments. Abbreviations: RTK, receptor tyrosine kinase; SE, standard error.

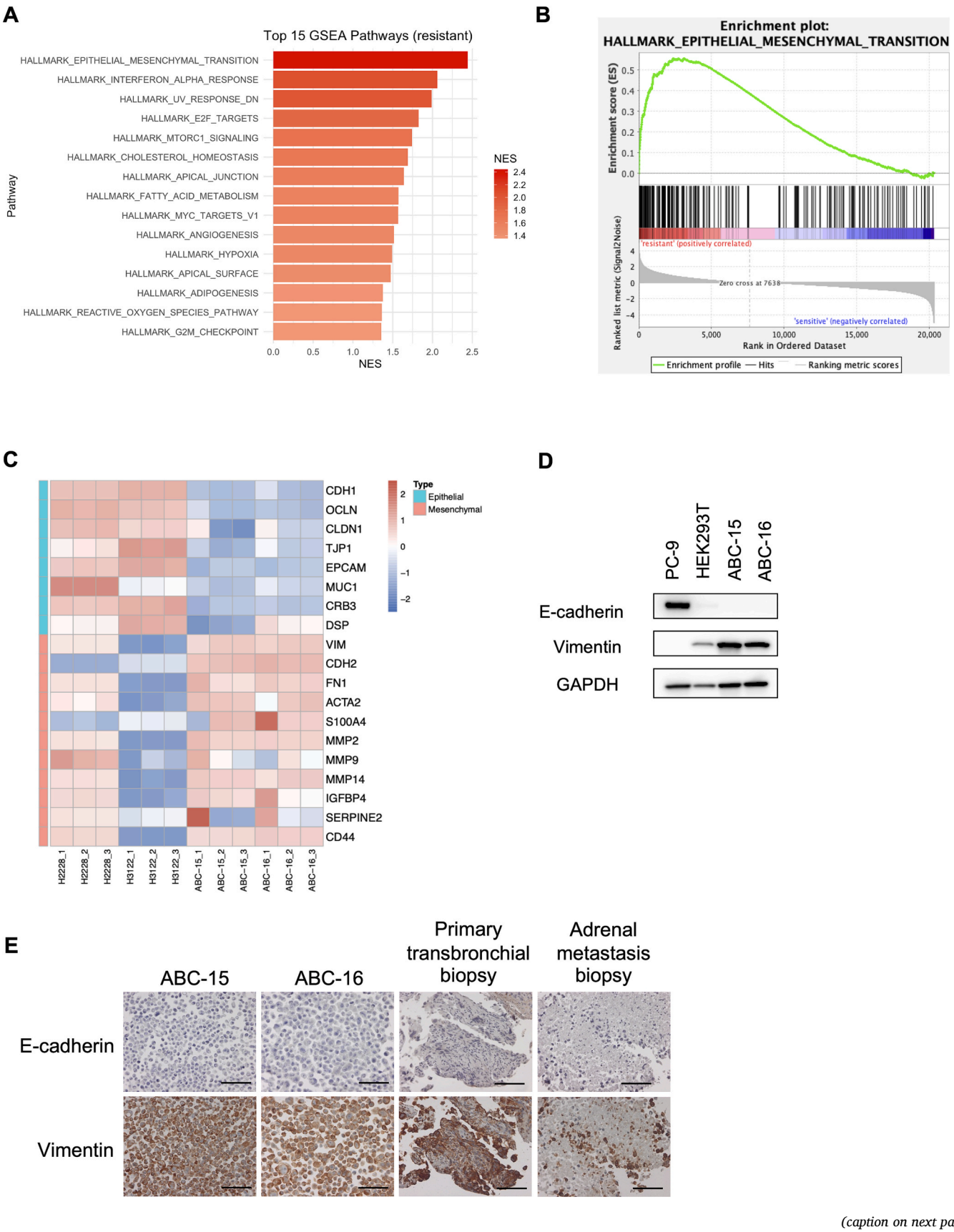

(caption on next page)

Fig. 3. EMT-associated features in ALK-TKI-resistant ABC-15 and ABC-16 cells. A. RNA sequencing was performed on ALK-TKI-sensitive cell lines (H2228 and H3122) and ALK-TKI-resistant (ABC-15 and ABC-16) cell lines. Gene set enrichment analysis (GSEA) using Hallmark gene sets from the Molecular Signatures Database (MSigDB) identified the 15 most significantly enriched pathways in resistant versus sensitive cell lines, ranked by normalized enrichment score (NES). B. GSEA enrichment plot of the HALLMARK_EPITHELIAL_MESENCHYMAL_TRANSITION gene set in resistant versus sensitive cell lines. C. Heatmap showing the expression of EMT-related genes in resistant and sensitive cell lines. Rows represent individual genes, and columns represent individual cell line samples. Epithelial and mesenchymal markers are indicated by the annotation bar on the left. The color scale represents row Z-score–normalized log2-transformed TPM expression values. D. Western blot analysis of EMT-associated proteins in ABC-15 and ABC-16 cells. PC-9 and HEK293T cells were included as control cell lines for EMT-marker expression. Experiments were performed independently three times with similar results. E. Immunohistochemistry for E-cadherin and vimentin in ABC-15 and ABC-16 cells, the primary transbronchial biopsy specimen obtained at diagnosis, and the adrenal metastasis biopsy specimen obtained during rapid disease progression on alectinib treatment. Scale bars: 100 μm. Abbreviations: GSEA, gene set enrichment analysis; IHC, immunohistochemistry; MSigDB, Molecular Signatures Database; NES, normalized enrichment score; TPM, transcripts per million.

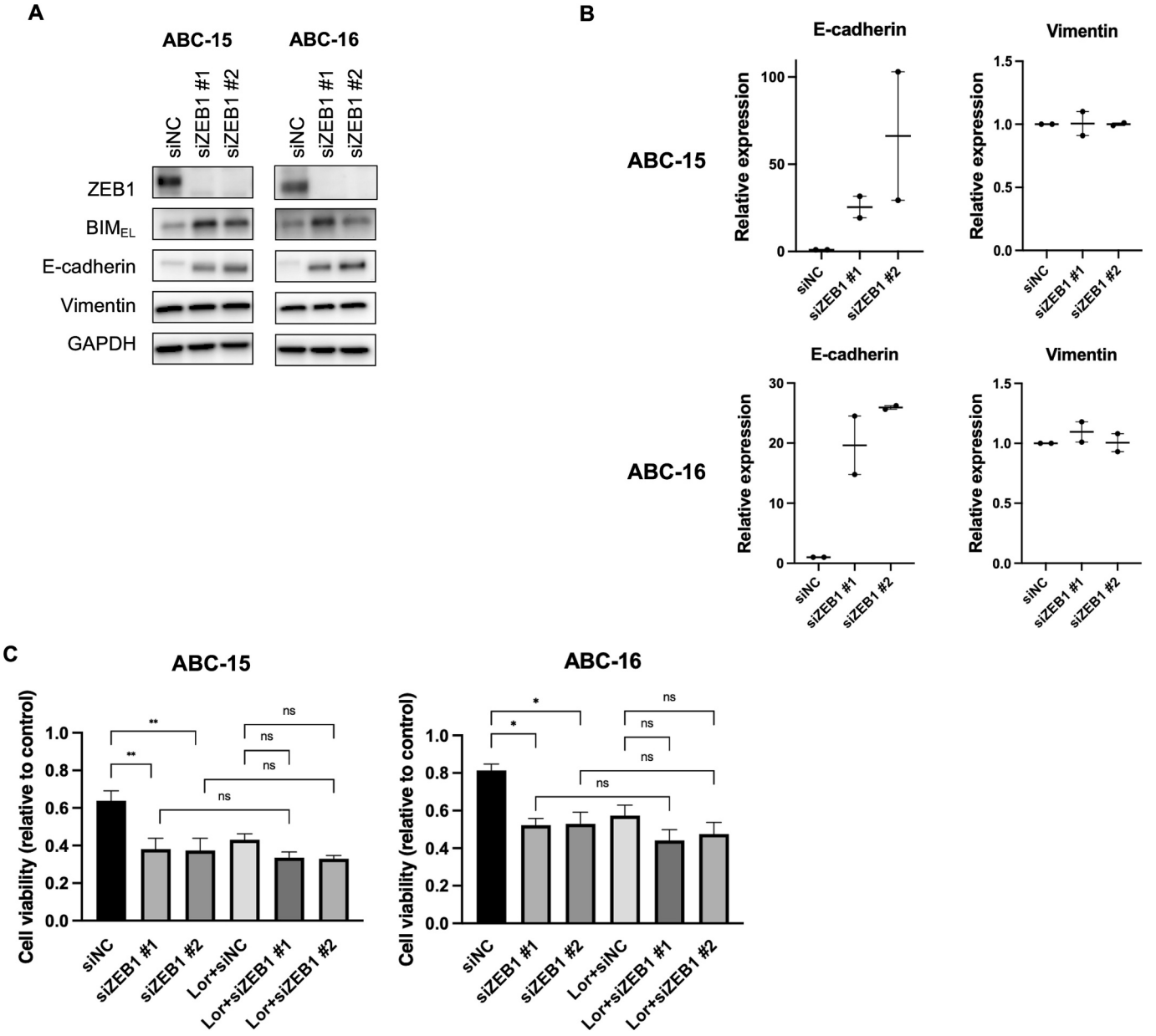

Fig. 4. Functional effects of ZEB1 knockdown in ABC-15 and ABC-16 cells. A. Western blot analysis of ZEB1, BIM, E-cadherin, and vimentin expression following ZEB1 knockdown in ABC-15 and ABC-16 cells. Cells were transfected with negative control siRNA (siNC) or two independent ZEB1-targeting siRNAs (#1 and #2). Experiments were independently repeated twice with similar results. B. RT-qPCR analysis of E-cadherin and vimentin mRNA expression following ZEB1 knockdown in ABC-15 and ABC-16 cells. Cells were transfected with siNC or two independent ZEB1-targeting siRNAs (#1 and #2). Relative expression levels were normalized to GAPDH. Data are presented as the mean ± SE of two independent experiments. C. MTT assay evaluating the effect of ZEB1 knockdown on lorlatinib sensitivity in ABC-15 and ABC-16 cells. Cells were transfected with siNC or two independent ZEB1-targeting siRNAs (#1 and #2) and treated with lorlatinib (1 μM) for 96 h. Cell viability is expressed relative to untreated control cells. Data are presented as the mean ± SE of three independent experiments. Statistical significance was evaluated using one-way ANOVA with Tukey's post hoc test. *$p < 0.05$, **$p < 0.01$; ns, not significant. Abbreviations: ANOVA, analysis of variance; SE, standard error; siNC, negative control small interfering RNA; siRNA, small interfering RNA.

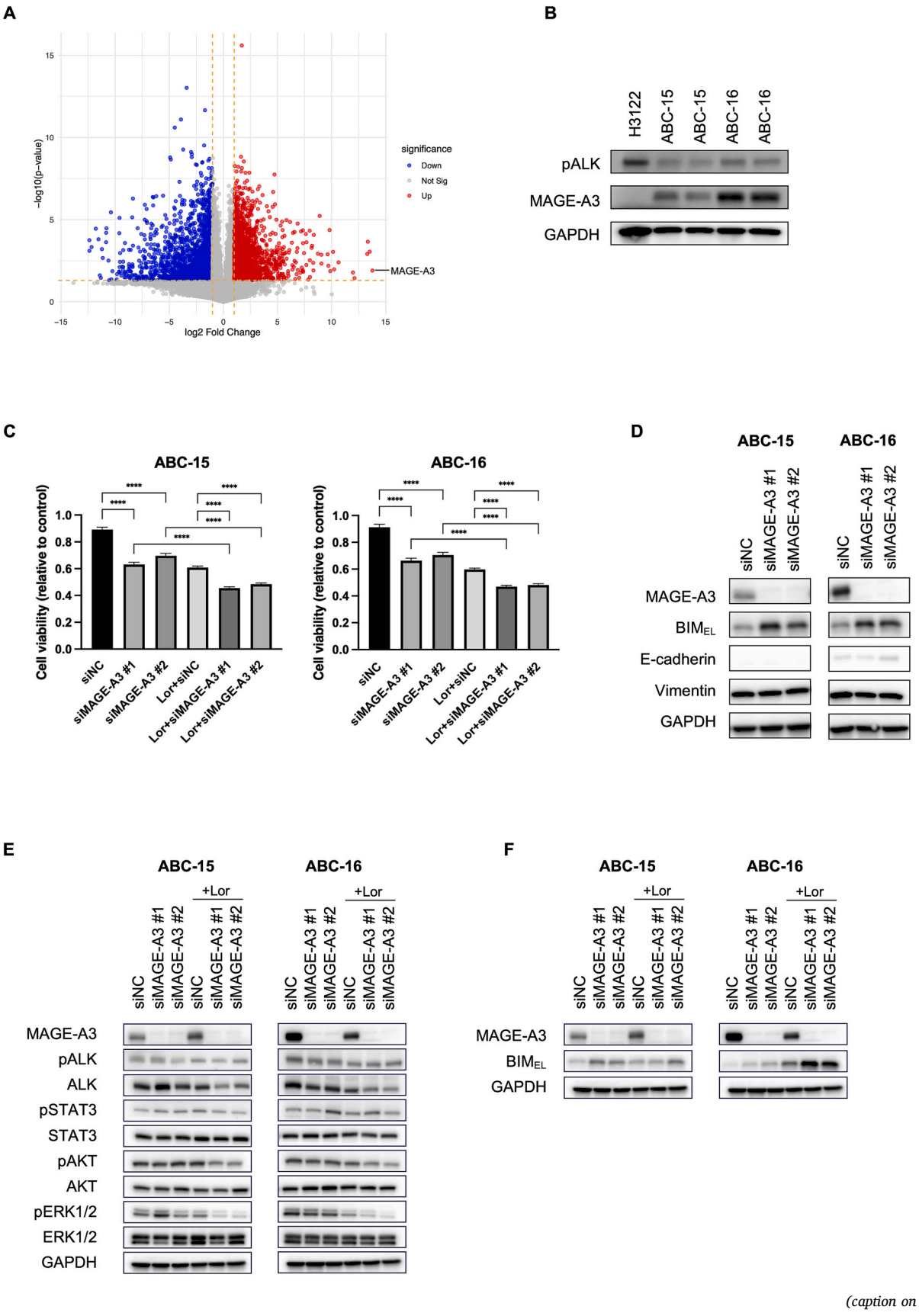

(caption on next page)

Fig. 5. Functional analysis of MAGE-A3 in ABC-15 and ABC-16 cells. A. Differential gene expression analysis comparing ALK-TKI-resistant (ABC-15 and ABC-16) cell lines with sensitive cell lines (H2228 and H3122). The volcano plot shows log2 fold change (x-axis) versus − log10 p-value (y-axis). Red and blue dots indicate significantly upregulated and downregulated genes, respectively, based on |log2 fold change| > 1 and $p < 0.05$, whereas gray dots represent genes that did not meet these significance thresholds. B. Western blot analysis of phosphorylated ALK (pALK) and MAGE-A3 protein levels in H3122, ABC-15, and ABC-16 cells. Two independent biological samples of ABC-15 and ABC-16 are shown. Experiments were independently repeated three times with similar results. C. MTT assay evaluating the effect of MAGE-A3 knockdown on lorlatinib sensitivity in ABC-15 and ABC-16 cells. Cells were transfected with siNC or two independent MAGE-A3-targeting siRNAs (#1 and #2) and treated with or without lorlatinib (1 μM) for 96 h. Cell viability is expressed relative to untreated siNC-transfected control cells. Data are presented as the mean ± SE of three independent experiments, each performed in triplicate. Statistical significance was evaluated using one-way ANOVA with Tukey's post hoc test. ****$p < 0.0001$. D. Western blot analysis of MAGE-A3, BIM, E-cadherin, and vimentin expression following MAGE-A3 knockdown in ABC-15 and ABC-16 cells. E. Western blot analysis of phosphorylated and total ALK, STAT3, AKT, and ERK1/2 after MAGE-A3 knockdown with or without lorlatinib treatment in ABC-15 and ABC-16 cells. F. Western blot analysis of MAGE-A3 and BIM expression after MAGE-A3 knockdown with or without lorlatinib treatment in ABC-15 and ABC-16 cells. For panels D–F, cells were transfected with siNC or two independent MAGE-A3-targeting siRNAs (#1 and #2). Where indicated, cells were treated with lorlatinib (1 μM) for 24 h. Experiments were independently repeated twice with similar results. Abbreviations: ANOVA, analysis of variance; SE, standard error; siNC, negative control small interfering RNA; siRNA, small interfering RNA. (For interpretation of the references to colour in this figure legend, the reader is referred to the web version of this article.)

beyond ALK-TKI monotherapy, with no statistically significant differences in phosphorylation of STAT3, AKT, or ERK1/2 between the two groups (Fig. 6C and Supplementary Fig. S6E). Cells treated with navitoclax showed a trend toward higher levels of cleaved PARP and cleaved caspase-3 in both cell lines, although no significant difference was observed between the monotherapy and combination treatments. Furthermore, statistical significance relative to the untreated control was achieved only for the cleaved caspase-3/caspase-3 ratio in ABC-15 cells (Fig. 6D). To further assess apoptosis induction, Annexin V/7-AAD flow cytometry was performed, revealing a significant increase in early apoptotic cells following treatment with the combination of lorlatinib and navitoclax (Fig. 6E).

We next evaluated the baseline expression of BCL-2 family proteins to assess whether ABC-15 and ABC-16 cells harbor molecular features that could confer susceptibility to navitoclax. ABC-15 and ABC-16 cells retained expression of BCL-2 and BCL-xL, direct targets of navitoclax, as well as MCL-1 (Supplementary Fig. S6F). In contrast, baseline BIM expression was lower in ABC-15 and ABC-16 cells, which showed higher ZEB1 expression, than in H2228/CHR1 cells. This expression profile, characterized by maintained BCL-2/BCL-xL expression alongside suppressed baseline BIM expression, suggests that apoptotic signaling may be regulated differently in these EMT-associated resistant cells than in non-EMT-resistant models. Such differential regulation may influence the susceptibility of these cells to BCL-2/BCL-xL inhibition.

Finally, the in vivo efficacy of this combination was evaluated using subcutaneous xenograft models derived from ABC-15 and ABC-16 cells. The mice received oral lorlatinib (10 mg/kg), navitoclax (80 mg/kg), or a combination of both. Although both monotherapies inhibited tumor growth, the combination treatment showed greater tumor growth suppression than either monotherapy without significant differences in body weight among the groups (Fig. 7).

4. Discussion

Alectinib is an established first-line therapy for ALK-positive NSCLC, based on the global ALEX and Japanese J-ALEX studies [4,6]. However, a subset of patients experiences rapid disease progression shortly after treatment initiation, representing an unresolved clinical challenge. Although the approved dose of alectinib in Japan used in the J-ALEX study (300 mg twice daily) differs from the global standard (600 mg twice daily), pharmacokinetic data demonstrate comparable systemic exposure [28]. Even with the third-generation ALK inhibitor lorlatinib, rapid disease progression persists in a minority of patients [29], suggesting an inherent limitation of ALK-TKI monotherapy. We established patient-derived cell lines from a patient who showed an initial radiological response followed by rapid disease progression within 1 month of alectinib initiation. EMT-associated features were observed in both the clinical specimens and the patient-derived cell lines. MAGE-A3 was identified as the most highly upregulated gene and was functionally implicated in the survival of resistant cells, independently of EMT regulation. Furthermore, the combination of an ALK-TKI and the BCL-2 family inhibitor navitoclax demonstrated enhanced antitumor activity both in vitro and in vivo.

Our patient exhibited an unusual clinical course characterized by a brief objective radiological response followed by rapid disease progression. A consensus definition of acquired resistance requires a sustained treatment response of at least 3–6 months to distinguish it from primary resistance, defined as a de novo lack of response [30,31].

Thus, the clinical course of our patient did not clearly fit either category, and we therefore describe it as rapid disease progression. In our patient, EMT-associated features were already present in the pre-treatment diagnostic specimen and were retained in the corresponding patient-derived resistant cell lines. This concordance suggests that these features were not solely attributable to culture-induced adaptation. Furthermore, given the rapid disease progression observed in our patient, our findings are consistent with the possibility that a pre-existing mesenchymal subpopulation contributed to the resistant phenotype, rather than with the de novo emergence of a mesenchymal phenotype during treatment. These findings support further investigation of pre-treatment EMT status, assessed by IHC or gene expression profiling, as a potential biomarker of rapid disease progression during ALK-TKI therapy.

The absence of both TTF-1 and Napsin A in the cell-block specimens, together with the poorly differentiated morphology and focal positivity for PAS, MUC1, and MUC5AC, may reflect reduced pulmonary epithelial differentiation with focal mucin-associated features. NKX2-1 (TTF-1) is a lineage-defining transcription factor that maintains pulmonary epithelial identity, and its loss can induce a shift toward gastric differentiation [32]. Consistent with this concept, experimental depletion of NKX2-1 in lung adenocarcinoma cells has been shown to downregulate alveolar differentiation genes, including *NAPSA*, which encodes Napsin A, while enriching EMT-associated transcriptional programs [33]. ABC-15 and ABC-16 cells exhibited prominent EMT-associated features, suggesting that attenuated lineage differentiation and the mesenchymal phenotype may coexist. Although these previous findings may help explain the TTF-1/Napsin A-negative phenotype in our models, we did not directly assess lineage transition and therefore cannot establish a causal relationship between this marker profile and EMT.

EMT is a well-recognized phenotypic resistance mechanism associated with drug tolerance, invasion, metastasis, and immune evasion [34]. RNA sequencing followed by GSEA showed enrichment of EMT-associated transcriptional programs in resistant ABC-15 and ABC-16 cells. Complementary analyses using KEGG, Reactome, Gene Ontology, and C2 curated gene sets consistently identified EMT-related signatures across multiple databases. In contrast, apoptosis-, hypoxia-, TGF-β-, and inflammation-related pathways were less consistently enriched (Supplementary Table S2). Both ABC-15 and ABC-16 cells harbored a *TP53* frameshift mutation (c.997dupC) accompanied by reduced p53 protein expression. Previous studies have shown that loss of p53 function can promote EMT through dysregulation of the miR-200/

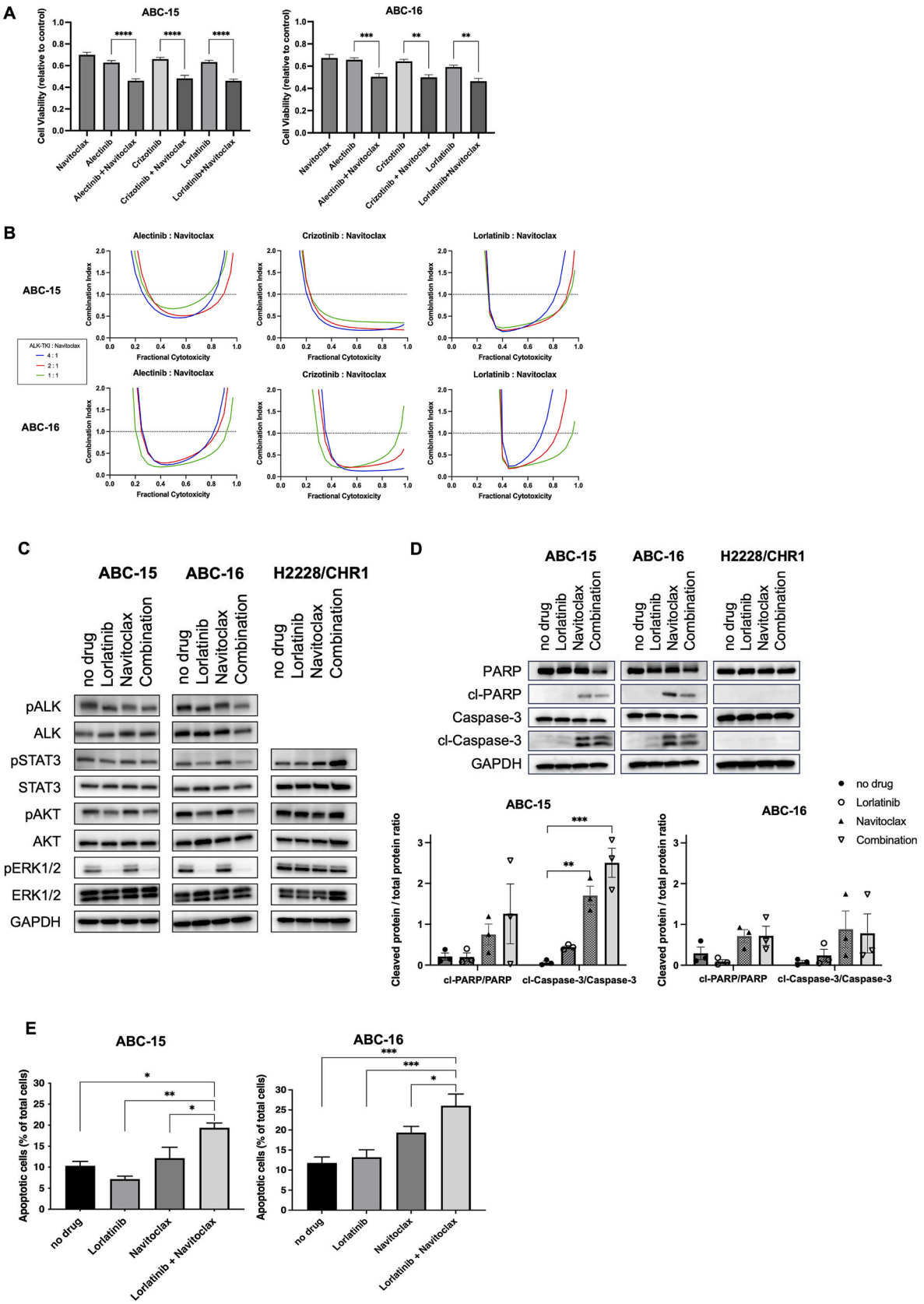

(caption on next page)

Fig. 6. Combination effects of ALK-TKIs and navitoclax in ABC-15 and ABC-16 cells with EMT-associated features. A. MTT assay evaluating the effects of combining ALK-TKIs with navitoclax in ABC-15 and ABC-16 cells. Cells were treated with alectinib, crizotinib, or lorlatinib (1 μM each) in the absence or presence of navitoclax (500 nM) for 96 h. Cell viability is expressed relative to untreated control cells. Data are presented as the mean ± SE of three independent experiments, each performed in triplicate. Statistical significance was evaluated using one-way ANOVA with Tukey's post hoc test. $^{**}p < 0.01$, $^{***}p < 0.001$, $^{****}p < 0.0001$. B. Median-effect plot analysis of ALK-TKI and navitoclax combinations in ABC-15 and ABC-16 cells. Combination index (CI) values were calculated using the Chou-Talalay method. Fixed drug ratios of ALK-TKI to navitoclax were 4:1, 2:1, and 1:1. C. Western blot analysis of phosphorylated and total ALK, STAT3, AKT, and ERK1/2 following treatment with lorlatinib and/or navitoclax in ABC-15, ABC-16, and H2228/CHR1 cells. Cells were treated with lorlatinib (1 μM), navitoclax (500 nM), or the combination for 6 h. Experiments were independently repeated three times with similar results. D. Western blot analysis of apoptosis-related proteins following treatment with lorlatinib and/or navitoclax in ABC-15, ABC-16, and H2228/CHR1 cells. Cells were treated with lorlatinib (1 μM), navitoclax (500 nM), or the combination for 24 h. Quantification of the cleaved PARP/PARP and cleaved caspase-3/caspase-3 ratios is shown in the lower panels. Data are presented as the mean ± SE of three independent experiments. Statistical significance was evaluated using one-way ANOVA with Tukey's post hoc test. $^{**}p < 0.01$, $^{***}p < 0.001$. The absence of significance markers indicates no statistically significant difference. E. Early apoptotic cells were quantified by flow cytometry using Annexin V/7-AAD staining in ABC-15 and ABC-16 cells treated with lorlatinib (1 μM), navitoclax (500 nM), or the combination for 72 h. Data are presented as the mean ± SE of three independent experiments. Statistical significance was evaluated using one-way ANOVA with Tukey's post hoc test. $^{*}p < 0.05$, $^{**}p < 0.01$, $^{***}p < 0.001$. Abbreviations: 7-AAD, 7-aminoactinomycin D; ANOVA, analysis of variance; CI, combination index; SE, standard error.

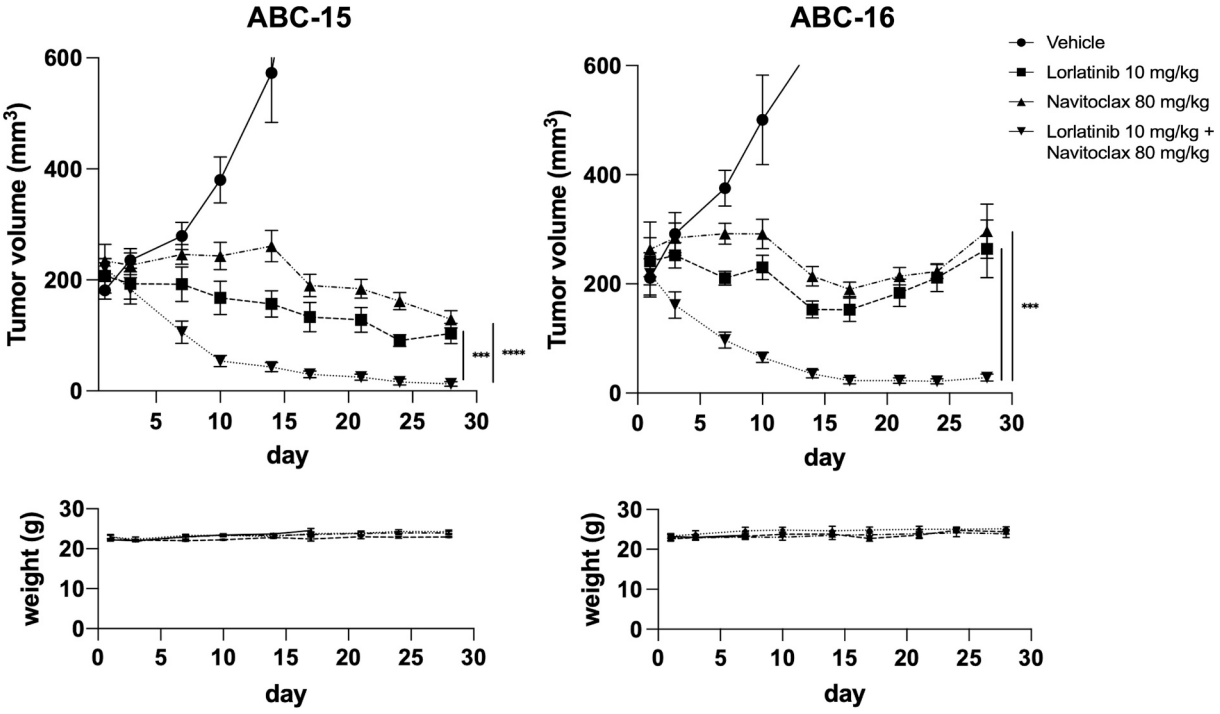

Fig. 7. In vivo antitumor effects of lorlatinib and navitoclax in ABC-15 and ABC-16 xenograft models. ABC-15 and ABC-16 cells were implanted subcutaneously into nude mice, followed by oral administration of lorlatinib (10 mg/kg) and/or navitoclax (80 mg/kg) five times per week for 4 weeks. Tumor growth was evaluated using 6–8 tumors from 3 to 4 mice per treatment group in the ABC-15 model and 10–12 tumors from 5 to 6 mice per treatment group in the ABC-16 model; mice in both models bore bilateral xenografts. Body weight was analyzed on a per-mouse basis. Data are presented as the mean ± SE. Statistical significance at the final time point was evaluated using one-way ANOVA with Tukey's post hoc test. $^{***}p < 0.001$, $^{****}p < 0.0001$. Abbreviations: ANOVA, analysis of variance; SE, standard error.

ZEB1 axis [26], suggesting that TP53 dysfunction may have contributed to the EMT-associated phenotype observed in our resistant models. In addition, co-occurring TP53 mutations have been associated with shorter progression-free and overall survival in patients with ALK-rearranged NSCLC receiving systemic therapy, including ALK-TKIs [35]. TP53 dysfunction has also been linked to chromosomal instability and recurrent amplification of oncogenic drivers such as MYC in ALK-rearranged tumors [36]. Therefore, TP53 dysfunction may have contributed to the poor response to ALK-TKIs through mechanisms beyond EMT, although these mechanisms were not directly examined in our models.

Several studies have linked EMT phenotypes to ALK-TKI resistance in ALK-positive NSCLC. Gainor et al. identified mesenchymal features in a subset of ALK inhibitor-resistant biopsy samples [10]. Fukuda et al. demonstrated that EMT and secondary ALK mutations can coexist as independent resistance mechanisms within a single tumor and that secondary mutations were detected almost exclusively in epithelial-type rather than mesenchymal-type tumor cells [14]. Consistent with this finding, no secondary *ALK* mutations were detected in our resistant ABC-15 and ABC-16 cell lines, which exhibited EMT-associated features. Furthermore, because EMT status can be adaptively modulated by tumor microenvironmental factors [37], these phenotypic features can be present in treatment-naive tumors, as observed in our case, as well as in tumors exposed to multiple lines of therapy [38]. Tanimura et al. demonstrated that mesenchymal features promote the emergence of ALK-TKI-tolerant cells and reported that pretreatment vimentin expression correlates with poorer clinical outcomes during ALK-TKI therapy [39]. Urbanska et al. also described EMT-associated resistance and rapid terminal progression during sequential ALK-TKI treatment [38]. Collectively, these findings are consistent with the possibility that pre-existing mesenchymal cell populations contributed to the rapid disease progression observed in our patient. Such cells may have preferentially persisted or expanded under ALK inhibition.

These findings prompted us to investigate the functional

contribution of EMT-associated features to resistance. *ZEB1* is a well-established transcriptional repressor that drives mesenchymal transition [34], and its upregulation was confirmed in both resistant cell lines. *ZEB1* knockdown increased E-cadherin and reduced cell viability, accompanied by BIM induction (Fig. 4), indicating that EMT-associated programs contribute to the maintenance of resistant cell viability. Nevertheless, restoration of ALK-TKI sensitivity was only partial and did not reach statistical significance, suggesting that additional mechanisms operate in parallel in ABC-15 and ABC-16 cells. While a previous preclinical study demonstrated that *ZEB1* knockdown reversed ALK-TKI resistance in certain EMT-associated crizotinib-resistant cell lines [14], another study reported observations consistent with ours [40]. These disparate outcomes suggest that the relative dependence of resistant cells on ALK- or EMT-driven survival signaling may vary among individual ALK-TKI-resistant cases.

Our RNA sequencing analysis showed upregulation of MAGE-A3 together with enrichment of EMT-related gene sets in ABC-15 and ABC-16 cells. To our knowledge, a direct association between MAGE-A3 and *ALK*-rearranged NSCLC or ALK-TKI resistance has not been established. MAGE genes belong to the cancer/testis antigen family and are selectively expressed in various malignancies, where they have been implicated in tumor progression, immune evasion, and therapeutic resistance [41]. MAGE-A3 has been shown to suppress apoptosis through the regulation of BIM and related survival pathways in multiple myeloma models [27], and previous studies have also linked MAGE-A family proteins to EMT-associated phenotypes in other cancer types [42,43]. In our resistant models, MAGE-A3 knockdown alone significantly reduced cell viability and induced BIM expression. MAGE-A3 knockdown also significantly enhanced the growth-inhibitory effect of lorlatinib, suggesting that MAGE-A3 may contribute to resistant-cell survival independently of EMT-associated features.

Suppression of BIM, a key regulator of mitochondrial apoptosis, has been associated with resistance to oncogene-targeted therapies in NSCLC. BIM expression can be attenuated by genetic mechanisms, such as a common BIM deletion polymorphism, or by ZEB1-mediated transcriptional repression during EMT [24,44]. Consistent with these findings, ABC-15 and ABC-16 cells showed low baseline BIM expression and high ZEB1 expression while retaining BCL-2 and BCL-xL expression. Both BCL-2 and BCL-xL are direct targets of navitoclax, and EMT-associated resistant cells have been reported to depend on BCL-xL for survival [24,45]. This expression profile may therefore be associated with susceptibility to BCL-2/BCL-xL inhibition. Navitoclax enhanced the growth-inhibitory effect of ALK inhibition in ABC-15 and ABC-16 cells. In contrast, no clear combination effect was observed in H2228/CHR1 or ABC-14 cells, neither of which showed EMT-associated features. These findings suggest that navitoclax sensitivity may be associated with the apoptotic protein profile of EMT-associated resistant cells, although additional molecular determinants are likely to influence treatment response.

These findings raise the question of why navitoclax showed greater antitumor activity when combined with ALK inhibition than as a monotherapy. EMT is generally considered an ALK-independent resistance mechanism in ALK-positive NSCLC [16]. However, ABC-15 and ABC-16 cells retained partial sensitivity to ALK-TKIs, and treatment attenuated the phosphorylation of several downstream signaling molecules. Taken together, these findings suggest that EMT-associated ZEB1 upregulation and MAGE-A3 upregulation may each contribute to constrained BIM expression, thereby impairing apoptotic signaling and permitting resistant-cell survival during ALK inhibition. Although no direct functional link between MAGE-A3 expression and EMT-associated features was observed, knockdown of either ZEB1 or MAGE-A3 induced BIM and reduced cell viability, indicating that these distinct, and not mutually exclusive, mechanisms each constrain BIM-dependent apoptosis. However, MAGE-A3 knockdown, but not ZEB1 knockdown, significantly enhanced the growth-inhibitory effect of lorlatinib, indicating that their contributions to the response to ALK inhibition may differ. In cells retaining BCL-2 and BCL-xL expression, inhibition of these proteins by navitoclax may facilitate apoptosis during ALK inhibition. This complementary effect may contribute to the synergistic growth-inhibitory effect observed in vitro.

Several limitations should be acknowledged. First, this study was based on a single clinical case and the corresponding patient-derived cell line models, limiting the generalizability of our findings. Validation in patient-derived xenograft models, in addition to the cell line-derived xenograft models used in this study, may help clarify the contributions of tumor heterogeneity and the microenvironment to resistance. Second, the limited availability of archived tissue precluded comprehensive longitudinal DNA-level genomic analyses of the original tumor specimens. It also prevented evaluation of additional EMT-associated markers beyond E-cadherin and vimentin in the resistant tumor specimen. Furthermore, comprehensive DNA-based genomic profiling, including copy-number analysis and assessment of CDKN2A/B deletion, was not performed in the established patient-derived cell lines. This represents a limitation of the present study, as the potential contribution of CDKN2A/B loss or other genomic co-alterations to the aggressive clinical behavior and unfavorable response to ALK-TKI therapy cannot be excluded [46]. Third, although TGF-β and Wnt/β-catenin signaling were not clearly activated at the transcriptomic level, the upstream regulators of the EMT-associated phenotype remain unresolved. Fourth, although *ZEB1* and *MAGE-A3* knockdown experiments supported their functional relevance, the precise mechanistic relationship among ALK-TKI resistance, EMT-associated biology, and MAGE-A3 expression remains unresolved. Fifth, because only small biopsy specimens were available, overall tumor heterogeneity and the presence and proportion of spindle-cell or giant-cell components could not be reliably assessed according to the diagnostic criteria for pulmonary pleomorphic carcinoma [47,48]. Therefore, a diagnosis of pulmonary pleomorphic carcinoma could neither be definitively established nor completely excluded. Moreover, the additional pathological findings from the patient-derived cell lines were insufficient to determine the histological subtype of the original tumor specimens. Finally, although our preclinical results demonstrated the antitumor activity of ALK-TKI plus navitoclax, the known toxicity of navitoclax, particularly thrombocytopenia, necessitates careful risk management and biomarker-guided patient selection for future clinical translation. Nevertheless, our findings provide a basis for future investigation of EMT-associated resistance and apoptosis-targeted therapeutic strategies in ALK-positive NSCLC.

In conclusion, our findings suggest that pre-existing mesenchymal subpopulations may contribute to rapid disease progression in a subset of patients with ALK-positive NSCLC treated with alectinib. MAGE-A3 upregulation and EMT-associated impairment of apoptotic signaling may contribute to therapeutic vulnerability in these resistant models. These results support the combination of an ALK-TKI and navitoclax as a promising strategy for overcoming this clinically challenging resistance phenotype.

CRediT authorship contribution statement

Tomoka Nishimura: Writing – review & editing, Writing – original draft, Visualization, Validation, Project administration, Methodology, Investigation, Formal analysis, Data curation, Conceptualization. **Shuta Tomida:** Writing – review & editing, Formal analysis. **Tadahiro Kuribayashi:** Writing – review & editing, Investigation. **Takaaki Tanaka:** Writing – review & editing, Investigation. **Taku Noumi:** Writing – review & editing, Investigation. **Masataka Taoka:** Writing – review & editing, Investigation. **Shunta Mori:** Writing – review & editing, Investigation. **Jun Nishimura:** Writing – review & editing, Investigation. **Ayako Morita:** Writing – review & editing, Investigation. **Kenji Takada:** Writing – review & editing, Investigation. **Naofumi Hara:** Writing – review & editing, Resources. **Hiromi Watanabe:** Writing – review & editing, Investigation. **Kiichiro Ninomiya:** Writing – review & editing, Resources. **Hisao Higo:** Writing – review & editing, Resources.

Toshio Kubo: Writing – review & editing, Resources. **Kammei Rai:** Writing – review & editing, Resources. **Eiki Ichihara:** Writing – review & editing, Resources. **Kadoaki Ohashi:** Writing – review & editing, Supervision, Resources, Funding acquisition, Conceptualization, Methodology. **Katsuyuki Hotta:** Writing – review & editing, Resources. **Yoshinobu Maeda:** Writing – review & editing, Supervision, Resources. **Yosuke Togashi:** Writing – review & editing, Supervision, Resources. **Go Makimoto:** Writing – review & editing, Visualization, Supervision, Resources, Project administration, Methodology, Funding acquisition, Formal analysis, Conceptualization.

Ethics declaration

Studies in human

This study was performed in compliance with relevant laws, regulatory frameworks and guidelines where the research took place.

This study was approved by the Institutional Review Board of Okayama University.

(Approval No. 1603-066).

Written informed consent to take part in the study and to publish the article has been obtained from all participants or their legal representatives. The privacy rights of participants have been observed.

This study included organ or tissue donors.

This study includes human biological material and consent was obtained by donors, or their next of kin or legal representatives, for use in this study and for publication of the article. The samples used in this research were not sourced from executed prisoners or prisoners of conscience.

This study was conducted in accordance with the following guidelines for animal welfare and/or reporting: the Policy on the Care and Use of the Laboratory Animals, Okayama University.

This study was approved by the Animal Care and Use Committee of Okayama University.

(Approval No. OKU-2023619).

Declaration of generative AI and AI-assisted technologies in the manuscript preparation process

During the preparation of this work, the authors used ChatGPT (OpenAI, San Francisco, CA, USA) to improve the clarity and readability of the manuscript. After using this tool, the authors reviewed and edited the content as needed and take full responsibility for the content of this publication.

Funding information

This work was supported by the Japan Society for the Promotion of Science Grant-in-Aid for Early-Career Scientists (22K16173 and 25K19440, G. Makimoto), the Okayama Health Foundation Cancer Research Grant (G. Makimoto), the Ryobi Teien Memory Foundation (G. Makimoto), the Teraoka Memorial Scholarship Foundation (G. Makimoto), and the Grant for Lung Cancer Research from the Japan Lung Cancer Society (provided to G. Makimoto in 2025 and K. Ohashi in 2017).

Declaration of competing interest

The authors declare the following financial interests/personal relationships which may be considered as potential competing interests: S. Tomida reports receiving a research grant from Illumina outside the submitted work. K. Ninomiya reports receiving honoraria from AstraZeneca, Boehringer Ingelheim, Kyowa Kirin, Eli Lilly Japan, Chugai Pharmaceutical, Nippon Kayaku, Taiho Pharmaceutical, MSD, Ono Pharmaceutical, Takeda Pharmaceutical, Pfizer, Bristol Myers Squibb, Elekta, Janssen, Daiichi Sankyo, Amgen, Novartis, and Guardant Health Japan outside the submitted work. E. Ichihara reports receiving honoraria from AstraZeneca, Novartis, Janssen, Chugai Pharmaceutical, Eli Lilly Japan, Pfizer, Bristol Myers Squibb, Ono Pharmaceutical, Takeda Pharmaceutical, and Boehringer Ingelheim, and research funding from Janssen outside the submitted work. K. Ohashi reports receiving honoraria from AstraZeneca, Pfizer, and Novartis; grants from Boehringer Ingelheim, Chugai Pharmaceutical, Eli Lilly Japan, Daiichi Sankyo, and Amgen; and research reagents from Genentech and Novartis outside the submitted work. K. Hotta reports receiving honoraria from AstraZeneca, Chugai Pharmaceutical, Eli Lilly Japan, MSD, Bristol Myers Squibb, Ono Pharmaceutical, Boehringer Ingelheim, Nippon Kayaku, Amgen, Taiho Pharmaceutical, Merck Biopharma, Janssen, and Takeda Pharmaceutical, and research funding from MSD, AstraZeneca, Eli Lilly Japan, Bristol Myers Squibb, AbbVie, Janssen, and Ono Pharmaceutical outside the submitted work. Y. Togashi reports receiving honoraria from Ono Pharmaceutical, Bristol Myers Squibb, Chugai Pharmaceutical, AstraZeneca, Eisai, and MSD, and research grants from Daiichi Sankyo, Janssen, AstraZeneca, KORTUC, Takeda Pharmaceutical, and Taiho Pharmaceutical outside the submitted work. G. Makimoto reports receiving honoraria from MSD, Chugai Pharmaceutical, Novartis Pharma, Ono Pharmaceutical, Bristol Myers Squibb, and Taiho Pharmaceutical outside the submitted work. The remaining authors declare no potential conflicts of interest.

Acknowledgments

The authors thank the patient and her family for their generous cooperation with this study. We thank Dr. Hiroyuki Yanai (Professor, Department of Pathology, Okayama University Graduate School of Medicine, Dentistry and Pharmaceutical Sciences) for the pathological re-evaluation of the clinical specimens and for valuable advice on the pathological interpretation of this case. We also thank Ms. Hiromi Nakashima and Ms. Kyoko Maeda of the Department of Hematology, Oncology, and Respiratory Medicine, Okayama University Graduate School of Medicine, Dentistry, and Pharmaceutical Sciences, for their excellent technical assistance. We would also like to thank Editage (www.editage.jp) for English language editing.

Appendix A. Supplementary data

Supplementary data to this article can be found online at https://doi.org/10.1016/j.lungcan.2026.109681.

References

[1] F. Bray, M. Laversanne, H. Sung, J. Ferlay, R.L. Siegel, I. Soerjomataram, A. Jemal, Global cancer statistics 2022: GLOBOCAN estimates of incidence and mortality worldwide for 36 cancers in 185 countries, CA Cancer J. Clin. 74 (3) (2024) 229–263.

[2] A.A. Thai, B.J. Solomon, L.V. Sequist, J.F. Gainor, R.S. Heist, Lung cancer, Lancet 398 (10299) (2021) 535–554.

[3] J.L. Schneider, J.J. Lin, A.T. Shaw, ALK-positive lung cancer: a moving target, Nat Cancer 4 (3) (2023) 330–343.

[4] S. Peters, D.R. Camidge, A.T. Shaw, S. Gadgeel, J.S. Ahn, D.W. Kim, S.I. Ou, M. Perol, R. Dziadziuszko, R. Rosell, A. Zeaiter, E. Mitry, S. Golding, B. Balas, J. Noe, P.N. Morcos, T. Mok, A.T. Investigators, Alectinib versus Crizotinib in Untreated ALK-Positive Non-Small-Cell Lung Cancer, N. Engl. J. Med. 377 (9) (2017) 829–838.

[5] T. Mok, D.R. Camidge, S.M. Gadgeel, R. Rosell, R. Dziadziuszko, D.W. Kim, M. Perol, S.I. Ou, J.S. Ahn, A.T. Shaw, W. Bordogna, V. Smoljanovic, M. Hilton, T. Ruf, J. Noe, S. Peters, Updated overall survival and final progression-free survival data for patients with treatment-naive advanced ALK-positive non-small-cell lung cancer in the ALEX study, Ann. Oncol. 31 (8) (2020) 1056–1064.

[6] T. Hida, H. Nokihara, M. Kondo, Y.H. Kim, K. Azuma, T. Seto, Y. Takiguchi, M. Nishio, H. Yoshioka, F. Imamura, K. Hotta, S. Watanabe, K. Goto, M. Satouchi, T. Kozuki, T. Shukuya, K. Nakagawa, T. Mitsudomi, N. Yamamoto, T. Asakawa, R. Asabe, T. Tanaka, T. Tamura, Alectinib versus crizotinib in patients with ALK-positive non-small-cell lung cancer (J-ALEX): an open-label, randomised phase 3 trial, Lancet 390 (10089) (2017) 29–39.

[7] K. Nakagawa, T. Hida, H. Nokihara, M. Morise, K. Azuma, Y.H. Kim, T. Seto, Y. Takiguchi, M. Nishio, H. Yoshioka, T. Kumagai, K. Hotta, S. Watanabe, K. Goto, M. Satouchi, T. Kozuki, R. Koyama, T. Mitsudomi, N. Yamamoto, T. Asakawa,

M. Hayashi, W. Hasegawa, T. Tamura, Final progression-free survival results from the J-ALEX study of alectinib versus crizotinib in ALK-positive non-small-cell lung cancer, Lung Cancer 139 (2020) 195–199.
[8] J. Rotow, T.G. Bivona, Understanding and targeting resistance mechanisms in NSCLC, Nat. Rev. Cancer 17 (11) (2017) 637–658.
[9] A.J. Cooper, L.V. Sequist, J.J. Lin, Third-generation EGFR and ALK inhibitors: mechanisms of resistance and management, Nat. Rev. Clin. Oncol. 19 (8) (2022) 499–514.
[10] J.F. Gainor, L. Dardaei, S. Yoda, L. Friboulet, I. Leshchiner, R. Katayama, I. Dagogo-Jack, S. Gadgeel, K. Schultz, M. Singh, E. Chin, M. Parks, D. Lee, R.H. DiCecca, E. Lockerman, T. Huynh, J. Logan, L.L. Ritterhouse, L.P. Le, A. Muniappan, S. Digumarthy, C. Channick, C. Keyes, G. Getz, D. Dias-Santagata, R.S. Heist, J. Lennerz, L.V. Sequist, C.H. Benes, A.J. Iafrate, M. Mino-Kenudson, J. A. Engelman, A.T. Shaw, Molecular Mechanisms of Resistance to First- and Second-Generation ALK Inhibitors in ALK-Rearranged Lung Cancer, Cancer Discov. 6 (10) (2016) 1118–1133.
[11] I. Dagogo-Jack, S. Yoda, J.K. Lennerz, A. Langenbucher, J.J. Lin, M.M. Rooney, K. Prutisto-Chang, A. Oh, N.A. Adams, B.Y. Yeap, E. Chin, A. Do, H.D. Marble, S. E. Stevens, S.R. Digumarthy, A. Saxena, R.J. Nagy, C.H. Benes, C.G. Azzoli, M. S. Lawrence, J.F. Gainor, A.T. Shaw, A.N. Hata, MET Alterations are a Recurring and Actionable Resistance Mechanism in ALK-Positive Lung Cancer, Clin. Cancer Res. 26 (11) (2020) 2535–2545.
[12] M. Miyawaki, H. Yasuda, T. Tani, J. Hamamoto, D. Arai, K. Ishioka, K. Ohgino, S. Nukaga, T. Hirano, I. Kawada, K. Naoki, Y. Hayashi, T. Betsuyaku, K. Soejima, Overcoming EGFR Bypass Signal-Induced acquired Resistance to ALK Tyrosine Kinase Inhibitors in ALK-Translocated Lung Cancer, Mol. Cancer Res. 15 (1) (2017) 106–114.
[13] N. Takegawa, H. Hayashi, N. Iizuka, T. Takahama, H. Ueda, K. Tanaka, M. Takeda, K. Nakagawa, Transformation of ALK rearrangement-positive adenocarcinoma to small-cell lung cancer in association with acquired resistance to alectinib, Ann. Oncol. 27 (5) (2016) 953–955.
[14] K. Fukuda, S. Takeuchi, S. Arai, R. Katayama, S. Nanjo, A. Tanimoto, A. Nishiyama, T. Nakagawa, H. Taniguchi, T. Suzuki, T. Yamada, H. Nishihara, H. Ninomiya, Y. Ishikawa, S. Baba, K. Takeuchi, A. Horiike, N. Yanagitani, M. Nishio, S. Yano, Epithelial-to-Mesenchymal transition is a Mechanism of ALK Inhibitor Resistance in Lung Cancer Independent of *ALK* Mutation Status, Cancer Res. 79 (7) (2019) 1658–1670.
[15] A.N. Hata, M.J. Niederst, H.L. Archibald, M. Gomez-Caraballo, F.M. Siddiqui, H. E. Mulvey, Y.E. Maruvka, F. Ji, H.E. Bhang, V. Krishnamurthy Radhakrishna, G. Siravegna, H. Hu, S. Raoof, E. Lockerman, A. Kalsy, D. Lee, C.L. Keating, D. A. Ruddy, L.J. Damon, A.S. Crystal, C. Costa, Z. Piotrowska, A. Bardelli, A. J. Iafrate, R.I. Sadreyev, F. Stegmeier, G. Getz, L.V. Sequist, A.C. Faber, J. A. Engelman, Tumor cells can follow distinct evolutionary paths to become resistant to epidermal growth factor receptor inhibition, Nat. Med. 22 (3) (2016) 262–269.
[16] J.J. Lin, G.J. Riely, A.T. Shaw, Targeting ALK: Precision Medicine takes on Drug Resistance, Cancer Discov. 7 (2) (2017) 137–155.
[17] G. Makimoto, K. Ohashi, S. Tomida, K. Nishii, T. Matsubara, H. Kayatani, H. Higo, K. Ninomiya, A. Sato, H. Watanabe, H. Kano, T. Ninomiya, T. Kubo, K. Rai, E. Ichihara, K. Hotta, M. Tabata, S. Toyooka, M. Takata, Y. Maeda, K. Kiura, Rapid Acquisition of Alectinib Resistance in ALK-Positive Lung Cancer with High Tumor Mutation Burden, J. Thorac. Oncol. 14 (11) (2019) 2009–2018.
[18] J. Hu, N. Ding, X. Xu, Y. Chen, Y. Zhang, J. Liu, J. Zhou, H. Bao, D. Zhang, Y. Song, Y. Shao, Y. Song, MET and NF2 alterations confer primary and early resistance to first-line alectinib treatment in ALK-positive non-small-cell lung cancer, Mol. Oncol. 19 (9) (2025) 2715–2729.
[19] H. Isozaki, E. Ichihara, N. Takigawa, K. Ohashi, N. Ochi, M. Yasugi, T. Ninomiya, H. Yamane, K. Hotta, K. Sakai, K. Matsumoto, S. Hosokawa, A. Bessho, T. Sendo, M. Tanimoto, K. Kiura, Non-Small Cell Lung Cancer Cells Acquire Resistance to the ALK Inhibitor Alectinib by Activating Alternative Receptor Tyrosine Kinases, Cancer Res. 76 (6) (2016) 1506–1516.
[20] K. Ninomiya, K. Ohashi, G. Makimoto, S. Tomida, H. Higo, H. Kayatani, T. Ninomiya, T. Kubo, E. Ichihara, K. Hotta, M. Tabata, Y. Maeda, K. Kiura, MET or NRAS amplification is an acquired resistance mechanism to the third-generation EGFR inhibitor naquotinib, Sci. Rep. 8 (1) (2018) 1955.
[21] International Agency for Research on Cancer, Detection of TP53 mutations by Sanger sequencing (IARC protocol, 2019 update), https://tp53.cancer.gov/pdf/TP53_SangerSequencing_NIH (14 July 2026) (2019).
[22] T.C. Chou, P. Talalay, A simple generalized equation for the analysis of multiple inhibitions of Michaelis-Menten kinetic systems, J. Biol. Chem. 252 (18) (1977) 6438–6442.
[23] T.C. Chou, Drug combination studies and their synergy quantification using the Chou-Talalay method, Cancer Res. 70 (2) (2010) 440–446.
[24] K.A. Song, M.J. Niederst, T.L. Lochmann, A.N. Hata, H. Kitai, J. Ham, K.V. Floros, M.A. Hicks, H. Hu, H.E. Mulvey, Y. Drier, D.A.R. Heisey, M.T. Hughes, N.U. Patel, E.L. Lockerman, A. Garcia, S. Gillepsie, H.L. Archibald, M. Gomez-Caraballo, T. J. Nulton, B.E. Windle, Z. Piotrowska, S.E. Sahingur, S.M. Taylor, M. Dozmorov, L. V. Sequist, B. Bernstein, H. Ebi, J.A. Engelman, A.C. Faber, Epithelial-to-Mesenchymal transition Antagonizes Response to Targeted Therapies in Lung Cancer by Suppressing BIM, Clin. Cancer Res. 24 (1) (2018) 197–208.
[25] H.Y. Zou, L. Friboulet, D.P. Kodack, L.D. Engstrom, Q. Li, M. West, R.W. Tang, H. Wang, K. Tsaparikos, J. Wang, S. Timofeevski, R. Katayama, D.M. Dinh, H. Lam, J.L. Lam, S. Yamazaki, W. Hu, B. Patel, D. Bezwada, R.L. Frias, E. Lifshits, S. Mahmood, J.F. Gainor, T. Affolter, P.B. Lappin, H. Gukasyan, N. Lee, S. Deng, R. K. Jain, T.W. Johnson, A.T. Shaw, V.R. Fantin, T. Smeal, PF-06463922, an ALK/ROS1 Inhibitor, Overcomes Resistance to first and Second Generation ALK Inhibitors in Preclinical Models, Cancer Cell 28 (1) (2015) 70–81.
[26] T. Kim, A. Veronese, F. Pichiorri, T.J. Lee, Y.J. Jeon, S. Volinia, P. Pineau, A. Marchio, J. Palatini, S.S. Suh, H. Alder, C.G. Liu, A. Dejean, C.M. Croce, p53 regulates epithelial-mesenchymal transition through microRNAs targeting ZEB1 and ZEB2, J. Exp. Med. 208 (5) (2011) 875–883.
[27] A.-H.-C. Mei, K. Tung, J. Han, D. Perumal, A. Laganà, J. Keats, D. Auclair, A. Chari, S. Jagannath, S. Parekh, H.J. Cho, MAGE-A inhibit apoptosis and promote proliferation in multiple myeloma through regulation of BIM and p21Cip1, Oncotarget 11 (7) (2020) 727–739.
[28] J.C. Hsu, F. Jaminion, E. Guerini, B. Balas, W. Bordogna, P.N. Morcos, N. Frey, Pharmacometric analyses of alectinib to facilitate approval of the optimal dose for the first-line treatment of anaplastic lymphoma kinase-positive non-small cell lung cancer, CPT Pharmacometrics Syst. Pharmacol. 10 (11) (2021) 1357–1370.
[29] A.T. Shaw, T.M. Bauer, F. de Marinis, E. Felip, Y. Goto, G. Liu, J. Mazieres, D. W. Kim, T. Mok, A. Polli, H. Thurm, A.M. Calella, G. Peltz, B.J. Solomon, C. T. Investigators, First-Line Lorlatinib or Crizotinib in Advanced ALK-Positive Lung Cancer, N. Engl. J. Med. 383 (21) (2020) 2018–2029.
[30] C.M. Lovly, P. Iyengar, J.F. Gainor, Managing Resistance to EFGR- and ALK-Targeted Therapies, Am. Soc. Clin. Oncol. Educ. Book 37 (2017) 607–618.
[31] D. Jackman, W. Pao, G.J. Riely, J.A. Engelman, M.G. Kris, P.A. Janne, T. Lynch, B. E. Johnson, V.A. Miller, Clinical definition of acquired resistance to epidermal growth factor receptor tyrosine kinase inhibitors in non-small-cell lung cancer, J. Clin. Oncol. 28 (2) (2010) 357–360.
[32] E.L. Snyder, H. Watanabe, M. Magendantz, S. Hoersch, T.A. Chen, D.G. Wang, D. Crowley, C.A. Whittaker, M. Meyerson, S. Kimura, T. Jacks, Nkx2-1 represses a latent gastric differentiation program in lung adenocarcinoma, Mol. Cell 50 (2) (2013) 185–199.
[33] J.L. Pulice, M. Meyerson, Amplified dosage of the NKX2-1 lineage transcription factor controls its oncogenic role in lung adenocarcinoma, Mol Cell 85(7) (2025) 1311-1329. e16.
[34] S. Lamouille, J. Xu, R. Derynck, Molecular mechanisms of epithelial-mesenchymal transition, Nat. Rev. Mol. Cell Biol. 15 (3) (2014) 178–196.
[35] A. Kron, C. Alidousty, M. Scheffler, S. Merkelbach-Bruse, D. Seidel, R. Riedel, M. A. Ihle, S. Michels, L. Nogova, J. Fassunke, C. Heydt, F. Kron, F. Ueckeroth, M. Serke, S. Kruger, C. Grohe, D. Koschel, J. Benedikter, B. Kaminsky, B. Schaaf, J. Braess, M. Sebastian, K.O. Kambartel, R. Thomas, T. Zander, A.M. Schultheis, R. Buttner, J. Wolf, Impact of TP53 mutation status on systemic treatment outcome in ALK-rearranged non-small-cell lung cancer, Ann. Oncol. 29 (10) (2018) 2068–2075.
[36] C. Alidousty, T. Baar, L.G. Martelotto, C. Heydt, S. Wagener, J. Fassunke, N. Duerbaum, A.H. Scheel, S. Frank, B. Holz, E. Binot, A. Kron, S. Merkelbach-Bruse, M.A. Ihle, J. Wolf, R. Buettner, A.M. Schultheis, Genetic instability and recurrent MYC amplification in ALK-translocated NSCLC: a central role of TP53 mutations, J. Pathol. 246 (1) (2018) 67–76.
[37] A. Kogita, Y. Togashi, H. Hayashi, S. Sogabe, M. Terashima, M.A. De Velasco, K. Sakai, Y. Fujita, S. Tomida, Y. Takeyama, K. Okuno, K. Nakagawa, K. Nishio, Hypoxia induces resistance to ALK inhibitors in the H3122 non-small cell lung cancer cell line with an ALK rearrangement via epithelial-mesenchymal transition, Int. J. Oncol. 45 (4) (2014) 1430–1436.
[38] E.M. Urbanska, J.B. Sorensen, L.C. Melchior, J.C. Costa, E. Santoni-Rugiu, Changing ALK-TKI-Resistance Mechanisms in Rebiopsies of ALK-Rearranged NSCLC: ALK- and BRAF-Mutations Followed by Epithelial-Mesenchymal transition, Int. J. Mol. Sci. 21 (8) (2020) 2847.
[39] K. Tanimura, T. Yamada, K. Okada, K. Nakai, M. Horinaka, Y. Katayama, K. Morimoto, Y. Ogura, T. Takeda, S. Shiotsu, K. Ichikawa, S. Watanabe, Y. Morimoto, M. Iwasaku, Y. Kaneko, J. Uchino, H. Taniguchi, K. Yoneda, S. Matoba, T. Sakai, H. Uehara, S. Yano, T. Kusaba, R. Katayama, K. Takayama, HER3 activation contributes toward the emergence of ALK inhibitor-tolerant cells in ALK-rearranged lung cancer with mesenchymal features, npj Precis. Oncol. 6 (1) (2022) 5.
[40] A. Gower, W.H. Hsu, S.T. Hsu, Y. Wang, G. Giaccone, EMT is associated with, but does not drive resistance to ALK inhibitors among EML4-ALK non-small cell lung cancer, Mol. Oncol. 10 (4) (2016) 601–609.
[41] J.L. Weon, P.R. Potts, The MAGE protein family and cancer, Curr. Opin. Cell Biol. 37 (2015) 1–8.
[42] X. Gao, G. Chen, H. Cai, X. Wang, K. Song, L. Liu, T. Qiu, Y. He, Aberrantly enhanced melanoma-associated antigen (MAGE)-A3 expression facilitates cervical cancer cell proliferation and metastasis via actuating Wnt signaling pathway, Biomed. Pharmacother. 122 (2020) 109710.
[43] H. Wang, M. Sang, C. Geng, F. Liu, L. Gu, B. Shan, MAGE-A is frequently expressed in triple negative breast cancer and associated with epithelial-mesenchymal transition, Neoplasma 63 (01) (2016) 44–56.
[44] K.P. Ng, A.M. Hillmer, C.T. Chuah, W.C. Juan, T.K. Ko, A.S. Teo, P.N. Ariyaratne, N. Takahashi, K. Sawada, Y. Fei, S. Soh, W.H. Lee, J.W. Huang, J.C. Allen Jr., X. Y. Woo, N. Nagarajan, V. Kumar, A. Thalamuthu, W.T. Poh, A.L. Ang, H.T. Mya, G. F. How, L.Y. Yang, L.P. Koh, B. Chowbay, C.T. Chang, V.S. Nadarajan, W.J. Chng, H. Than, L.C. Lim, Y.T. Goh, S. Zhang, D. Poh, P. Tan, J.E. Seet, M.K. Ang, N. M. Chau, Q.S. Ng, D.S. Tan, M. Soda, K. Isobe, M.M. Nothen, T.Y. Wong, A. Shahab, X. Ruan, V. Cacheux-Rataboul, W.K. Sung, E.H. Tan, Y. Yatabe, H. Mano, R.A. Soo, T.M. Chin, W.T. Lim, Y. Ruan, S.T. Ong, A common BIM deletion polymorphism mediates intrinsic resistance and inferior responses to tyrosine kinase inhibitors in cancer, Nat. Med. 18 (4) (2012) 521–528.
[45] A. Lopez, D.E. Reyna, N. Gitego, F. Kopp, H. Zhou, M.A. Miranda-Roman, L. U. Nordstrom, S.R. Narayanagari, P. Chi, E. Vilar, A. Tsirigos, E. Gavathiotis, Co-

targeting of BAX and BCL-XL proteins broadly overcomes resistance to apoptosis in cancer, Nat. Commun. 13 (1) (2022) 1199.
[46] L. Lara-Mejia, A.F. Cardona, L. Mas, C. Martin, S. Samtani, L. Corrales, G. Cruz-Rico, J. Remon, M. Galvez-Nino, R. Ruiz, E. Rios-Garcia, F. Tejada, N. Lozano-Vazquez, R. Rosell, O. Arrieta, Impact of concurrent Genomic Alterations on Clinical Outcomes in patients with ALK-Rearranged NSCLC, J. Thorac. Oncol. 19 (1) (2024) 119–129.
[47] A.G. Nicholson, M.S. Tsao, M.B. Beasley, A.C. Borczuk, E. Brambilla, W.A. Cooper, S. Dacic, D. Jain, K.M. Kerr, S. Lantuejoul, M. Noguchi, M. Papotti, N. Rekhtman, G. Scagliotti, P. van Schil, L. Sholl, Y. Yatabe, A. Yoshida, W.D. Travis, The 2021 WHO Classification of Lung Tumors: Impact of advances since 2015, J. Thorac. Oncol. 17 (3) (2022) 362–387.
[48] T. Sasaki, H. Kuno, T. Hiyama, S. Oda, S. Masuoka, Y. Miyasaka, T. Taki, Y. Nagasaki, S.J. Ohtani-Kim, G. Ishii, S. Kaku, G.S. Shroff, T. Kobayashi, 2021 WHO Classification of Lung Cancer: Molecular Biology Research and Radiologic-Pathologic Correlation, Radiographics 44 (3) (2024) e230136.